How accurate are the Minnesota density functionals for non-covalent interactions, isomerization energies, thermochemistry, and barrier heights involving molecules composed of main-group elements?

Narbe Mardirossian[†] and Martin Head-Gordon[*,†]

†*Kenneth S. Pitzer Center for Theoretical Chemistry, Department of Chemistry, University of California, Berkeley, California 94720, USA*
‡*Chemical Sciences Division, Lawrence Berkeley National Laboratory, Berkeley, California 94720, USA*

E-mail: mhg@cchem.berkeley.edu

Abstract

The 14 Minnesota density functionals published between the years 2005 and early 2016 are benchmarked on a comprehensive database of 4986 data points (84 datasets) involving molecules composed of main-group elements. The database includes non-covalent interactions, isomerization energies, thermochemistry, and barrier heights, as well as equilibrium bond lengths and equilibrium binding energies of non-covalent dimers. Additionally, the sensitivity of the Minnesota density functionals to the choice of basis set and integration grid is explored for both non-covalent interactions and thermochemistry.

Overall, the main strength of the hybrid Minnesota density functionals is that the best ones provide very good performance for thermochemistry (e.g. M06-2X), barrier heights (e.g. M08-HX, M08-SO, MN15), and systems heavily characterized by self-interaction error (e.g. M06-2X, M08-HX, M08-SO, MN15), while the main weakness is that none of them are state-of-the-art for the full spectrum of non-covalent interactions and isomerization energies (although M06-2X is recommended from the ten hybrid Minnesota functionals). Similarly, the main strength of the local Minnesota density functionals is that the best ones provide very good performance for thermochemistry (e.g. MN15-L), barrier heights (e.g. MN12-L), and systems heavily characterized by self-interaction error (e.g. MN12-L and MN15-L), while the main weakness is that none of them are state-of-the-art for the full spectrum of non-covalent interactions and isomerization energies (although M06-L is clearly the best from the four local Minnesota functionals). As an overall guide, M06-2X and MN15 are perhaps the most broadly useful hybrid Minnesota functionals, while M06-L and MN15-L are perhaps the most broadly useful local Minnesota functionals, although each has different strengths and weaknesses.

1 Introduction

Density functional theory (DFT) provides an in principle exact approach to the problem of electronic structure theory.[1] While the exact exchange-correlation functional is unknown, and approximate functionals continue to face

challenging problems,[2,3] tremendous progress has been made in developing practical functionals that offer good accuracy for many types of chemical problems at moderate computational cost. While functionals from the 1990s such as BLYP,[4,5] B3LYP,[4–6] PBE,[7] and PBE0[8] remain widely used (with a combined total of more than 200,000 citations), there has been a proliferation of new functionals in the past decade.

Specifically, since 2005, Truhlar and coworkers have published 14 highly-parameterized local (M06-L,[9] M11-L,[10] MN12-L,[11] and MN15-L[12]), global hybrid (M05,[13] M05-2X,[14] M06,[15] M06-2X,[15] M06-HF,[16] M08-HX,[17] M08-SO,[17] and MN15[18]), and range-separated hybrid (M11[19] and MN12-SX[20]) density functionals with kinetic energy density dependence. Of these 14 functionals, 10 have been of the meta-generalized gradient approximation (meta-GGA) variety, while 4 (MN12-SX, MN15, MN12-L, and MN15-L) have been of the meta-nonseparable gradient approximation (meta-NGA) variety. Table 1 contains a compact summary of the features of these 14 functionals, which are often designated as the "Minnesota" functionals.

Collectively, the Minnesota functionals are perhaps the most widely adopted of recently-developed functionals, with a combined total of more than 10,000 citations across the 12 published papers. However, since there are now 14 of them, the question naturally arises as to which is the best choice for chemical applications? That is the main question this work seeks to address. The answer may not be the obvious one, which is to use the most recent and most sophisticated functional that is computationally affordable for the task at hand. One reason is that the failures of semi-empirical density functionals vary for different classes of problems. For systems where strong correlation (SC) effects are important (multi-reference character: primarily a defect of the correlation functional), exact exchange leads to larger errors.[21] For systems where self-interaction error (SIE) is in play (odd electrons or charge-transfer excited states: primarily a defect of the exchange functional), more exact exchange typically reduces errors.[22]

A second reason is more subtle. More recent and more sophisticated Minnesota functional design (for instance the introduction of meta-NGAs) has been accompanied by the addition of many more empirical parameters. For the case of local functionals for example, one can compare the 34 parameters of M06-L against the 44 of M11-L against the 58 of MN12-L and MN15-L. The same trend can be seen for the hybrid functionals as well, increasing from 29 (M06-2X) to 47 (M08-HX) to 59 (MN15) parameters. Large increases in the number of parameters can lead to overfitting, which reduces predictive power.[23] Furthermore, published assessments of new Minnesota functionals upon introduction have largely been for datasets on which the parameters of each new functional were trained.[10–12,19,20] For example, M11-L was exclusively validated on its own training set upon publication, while MN15-L was tested on a set of only 56 data points, mostly consisting of solid state properties. Success on training datasets only confirms the flexibility of the functional form to fit the training data, but does not indicate accuracy when transferred to independent problems.

Finally, the inclusion of novel datasets in the training set of a semi-empirical density functional (such as those containing transition metals, solid-state properties, or multi-reference bond energies) can potentially extend its range of applicability (a clearly desirable attribute). However, it also has the potential of having a detrimental effect on the accuracy of a functional for conventional interactions. With the aim of achieving broader accuracy, the training sets for the most recent Minnesota functionals have been expanded in this direction, with the hope that a large improvement in these traditionally unexplored areas (e.g. multi-reference transition-metal bond energies) comes at the cost of minor loss in accuracy for typical datasets (e.g. closed-shell non-covalent interactions).

For reasons such as those given above, it is common to perform project-specific validation calculations using a variety of different functionals in order to make a final choice for applied DFT studies. This is a pragmatic strat-

egy, but has the limitation that the conclusions are usually non-transferable, because one reliable density functional is virtually never uniformly better than another. In order to draw more general conclusions about the relative virtues of the Minnesota functionals, it is essential to gather as much high quality test data together in one place as possible, and compare all 14 functionals against these reference values on an equal, unbiased footing. With results of statistical significance in hand, more general conclusions can be drawn. That is the goal of this paper.

After a qualitative description of the 14 Minnesota functionals, details regarding the calculations, as well as the 84 datasets used for the assessment, are given. In brief, the assessment database comprises nearly 5000 data points that have been culled from the benchmarking activities of numerous groups, including Hobza, Sherrill, Herbert, Grimme, Karton, and Martin. The reference data is typically estimated to be at least 10 times more accurate than the very best available density functionals, so that robust and meaningful conclusions can be drawn. The data points are divided into several categories: non-covalent interactions, isomerization energies, thermochemistry, barrier heights, and potential energy curves for non-covalent interactions. Within certain categories, the data points are further subdivided into easy cases versus difficult cases, where the latter should reflect a strong presence of one of the two aforementioned remaining shortcomings in modern density functionals – either strong correlation or self-interaction error. The performance of the Minnesota functionals is evaluated across all of these categories, and after considering the convergence of each functional with respect to basis set and integration grid, appropriate conclusions and recommendations are provided.

2 Minnesota Functionals

The complete equations and parameters defining the Minnesota functionals can be found in the citations provided in Table 1. Therefore, only a brief chronological review will be presented in this section in order to summarize the evolution of the various exchange and correlation functional forms that have been utilized since 2005. For further discussion of the Minnesota functionals, the reader may wish to consult a comprehensive review by Peverati and Truhlar.[24]

The exchange component of the first Minnesota functional, M05, used the PBE exchange functional[7] as its foundation and enhanced it with a 12-term power series inhomogeneity correction factor (ICF) in Becke's τ-dependent variable,[25] w. On the other hand, the correlation component of M05 was similar to that of B97[23] with two differences: the same-spin correlation functional utilized Becke's τ-dependent self-correlation correction (SCC) factor[26] and both power series had five terms instead of three. Furthermore, the two nonlinear correlation parameters ($\gamma_{c,ss}$ and $\gamma_{c,os}$) were reoptimized and all three uniform electron gas (UEG) limits were satisfied, resulting in a total of 22 fitted parameters (20 linear and 2 nonlinear), including the linear exact exchange mixing parameter (28%). The construction of M05-2X was identical to that of M05, except the exact exchange mixing parameter of M05 was doubled and fixed (56%) and the two nonlinear correlation parameters were borrowed from M05, for a total of 19 fitted parameters.

With M06-L, Zhao and Truhlar set out to develop an efficient, local meta-GGA functional. The functional form of M06-L was identical to that of an unhybridized M05 or M05-2X, with one exception: all three components (exchange, same-spin correlation, and opposite-spin correlation) had an additional, five-term, VSXC-type[27] ICF enhancing the associated UEG energy density. Since the nonlinear correlation parameters were again borrowed from M05, M06-L ended up with a total of 34 fitted parameters. M06-HF was designed primarily as a density functional for spectroscopy, and its construction was identical to that of a hybridized M06-L, with one exception: the fourth-order terms from the VSXC-type exchange ICF were dropped (two fewer parameters). Accordingly, M06-HF had a total of 32 fitted parameters, with a fixed exact exchange parameter of 100%.

The 2006 family of Minnesota functionals culminated with the M06 and M06-2X density functionals. The construction of the global hybrid M06 functional was identical to that of M06-HF, but the exact exchange parameter was allowed to relax to 27% (for a total of 33 fitted parameters). Employing the same "2X" strategy that accompanied the transition from M05 to M05-2X, M06-2X had double the amount of exact exchange (54%) as M06, and the entire VSXC-type exchange ICF was dropped, resulting in a functional with 29 fitted parameters.

The two Minnesota functionals from 2008, M08-HX and M08-SO, were substantially different from their predecessors with respect to both their exchange and correlation components. The exchange functionals were based on a weighted combination of the PBE and RPBE[28] exchange functionals, each of which were enhanced by separate 12-term power series ICFs in w. The correlation functionals no longer utilized the Stoll ansatz[29] (separation into same-spin and opposite-spin components) and Becke's SCC factor was dropped due to convergence problems. Instead, a third 12-term power series ICF in w enhanced the PW92 correlation functional[30] and a fourth one enhanced the PBE correlation functional gradient correction term. For M08-HX, only the two UEG limits were satisfied (47 fitted parameters), while for M08-SO, the gradient expansion to second order for both exchange and correlation was upheld, leading to three additional fixed parameters (44 fitted parameters). With M08-HX, the percentage of exact exchange was optimized to 52.23%, while with M08-SO, it was slightly larger at 56.79%.

In 2011, Peverati and Truhlar put forth two meta-GGA density functionals: M11 and M11-L. M11 was a range-separated (long-range-corrected) version of M08-SO, with the following differences: a constraint on the zeroth-order coefficient of the power series enhancing the PBE correlation functional gradient correction term was relaxed, two additional constraints for the exchange functional were enforced, and the last term from all four ICFs was dropped, resulting in 11-term power series ICFs. The coefficient of short-range exact exchange was optimized to 42.8%, as was the value of $\omega = 0.25$, giving M11 a total of 40 fitted parameters. The local meta-GGA density functional, M11-L, was developed as a potential successor to the widely-used M06-L functional. The exchange functional of M11-L included a novel "dual-range" partitioning, such that it contained a "local long-range" exchange contribution in addition to the local short-range exchange contribution that was borrowed from M11, while the correlation functional of M11-L was almost identical to that of M11. However, all six power series (two from short-range exchange, two from long-range exchange, and two from correlation) were modified to contain only nine terms each. With 54 linear parameters and a single nonlinear parameter ($\omega = 0.25$), eight constraints were placed on the exchange functional and three on the correlation functional, giving a total of 44 fitted parameters.

The first Minnesota meta-NGA density functionals (MN12-L and MN12-SX) were introduced in 2012. MN12-L was a local functional with an exchange component that not only depended on Becke's finite-domain-transformed $\nabla\rho$- and τ-dependent variables, u and w, but additionally on a new ρ-dependent variable, v. Its correlation functional was identical in form to the one used in M11-L. However, all constraints including the UEG ones were abandoned, and with 40 exchange parameters and 18 correlation parameters, MN12-L had a notably larger total of 58 parameters. MN12-SX was a 58-parameter, range-separated (screened-exchange) version of MN12-L, with the only difference being the additional, fixed parameters that were introduced as a result of the modification, namely 25% short-range exact exchange and $\omega = 0.11$ (borrowed from HSE06[31]). The functional form of the latest local Minnesota density functional, MN15-L, is identical to that of MN12-L, but trained on a larger dataset using some constraints imposed to prevent excessively large values of individual parameters. Finally, MN15, a global hybrid meta-NGA, is simply a hybridized version of MN15-L with 59 parameters. The expanded datasets used for the most recent functionals include a stronger representation of energetics that are challenging for

density functionals, including multi-reference transition-metal bond energies and transition-metal atomic excitation energies.

Table 1: Details for the 14 Minnesota density functionals. L stands for local, GH stands for global hybrid, and RSH stands for range-separated hybrid. The second column lists the number of parameters that were optimized on a training set for the given functional. The third column lists the percentage of exact exchange, $c_x \cdot 100$, as well as the value for ω in parentheses, if applicable. The column labeled UEG indicates whether or not the uniform electron gas limits were satisfied.

Functional	# (Fitted)	$c_x \cdot 100$ (ω)	Class	Rung	UEG	Ref.
M05	22	28	GH meta-GGA	4	Yes	13
M05-2X	19	56	GH meta-GGA	4	Yes	14
M06	33	27	GH meta-GGA	4	Yes	15
M06-2X	29	54	GH meta-GGA	4	Yes	15
M06-HF	32	100	GH meta-GGA	4	Yes	16
M08-HX	47	52.23	GH meta-GGA	4	Yes	17
M08-SO	44	56.79	GH meta-GGA	4	Yes	17
M11	40	42.8-100 (0.25)	RSH meta-GGA	4	Yes	19
MN12-SX	58	25-0 (0.11)	RSH meta-NGA	4	No	20
MN15	59	44	GH meta-NGA	4	No	18
M06-L	34	0	L meta-GGA	3	Yes	9
M11-L	44	0 (0.25)	L meta-GGA	3	Yes	10
MN12-L	58	0	L meta-NGA	3	No	11
MN15-L	58	0	L meta-NGA	3	No	12

3 Computational Details

The def2-QZVPPD basis set was used for all of the datasets without counterpoise corrections. The (99,590) grid (99 radial shells with 590 grid points per shell) was used for all of the datasets except AE18 and RG10. The (500,974) grid was used for both of these datasets. The SG-1 grid[32] was used to calculate the contribution from the VV10 nonlocal correlation functional[33] in all cases.

For the basis set limit tests involving non-covalent interactions, the (99,590) grid was used, while eight augmented basis sets from three different families were tested: the aug-cc-pVXZ (X=T,Q,5) Dunning basis sets,[34–36] the aug-pc-X (X=2,3,4) Jensen basis sets,[37–39] and the def2-XZVPPD (X=T,Q) Karlsruhe basis sets.[40–44] For the basis set limit tests involving thermochemistry, the (99,590) grid was used, while ten unaugmented basis sets from three different families were tested: the cc-pVXZ (X=D,T,Q) Dunning basis sets,[34–36] the pc-X (X=1,2,3,4) Jensen basis sets,[37–39] and the def2-SVP and def2-XZVPP (X=T,Q) Karlsruhe basis sets.[40–44]

For the integration grid limit tests involving non-covalent interactions, the def2-QZVPPD basis set was used, while nine different grids were tested, formed from the combination of three radial {99, 250, 500} and three angular {590, 770, 974} choices. For the integration grid limit tests involving thermochemistry, the def2-QZVPPD basis set was used, while five different grids were tested: SG-1, (50,194), (75,302), (99,590), and (500,974).

The database used to assess the Minnesota density functionals in this benchmark is constructed from 84 existing datasets and contains 4986 data points, requiring 5931 single-point calculations. 82 of these 84 datasets (AE18 and RG10 are excluded) are classified according to eight categories (or datatypes): NCED (non-covalent dimers (easy)), NCEC (non-covalent clusters (easy)), NCD (non-covalent dimers (difficult)), IE (isomerization energies (easy)), ID (isomerization energies (difficult)), TCE (thermochemistry (easy)), TCD (thermochemistry (difficult)), and BH (barrier heights). The number of data points (and datasets) in NCED, NCEC, NCD, IE, ID, TCE, TCD, and BH are 1744 (18), 243 (12), 91 (5), 755 (12), 155 (5), 947 (15), 258 (7), and 206 (8), respectively. Detailed information about the datasets can be found in Table 2, and general features of each category will be discussed in Section 4. All of the calculations were performed with a development version of Q-Chem 4.[45]

4 Database Results

4.1 Overall Performance for Energetics

Before focusing on the performance of the Minnesota density functionals for the 84 individual datasets, it is useful to consider Table 3 in order to understand how these functionals perform on the eight main datatypes that are being bench-

Table 2: Summary of the 84 datasets used to benchmark the Minnesota density functionals. The datatypes are explained in Section 3. The fifth column contains the root-mean-squares of the dataset reaction energies. PEC stands for potential energy curve, SR stands for single-reference, MR stands for multi-reference, Bz stands for benzene, Me stands for methane, and Py stands for pyridine.

Name	Datatype	#	Description	ΔE (kcal/mol)	Ref.
A24	NCED	24	Binding energies of small non-covalent complexes	2.65	46
DS14	NCED	14	Binding energies of complexes containing divalent sulfur	3.70	47
HB15	NCED	15	Binding energies of hydrogen-bonded dimers featuring ionic groups common in biomolecules	19.91	48
HSG	NCED	21	Binding energies of small ligands interacting with protein receptors	6.63	49,50
NBC10	NCED	184	PECs for BzBz (5), BzMe (1), MeMe (1), BzH_2S (1), and PyPy (2)	1.91	50–53
S22	NCED	22	Binding energies of hydrogen-bonded and dispersion-bound non-covalent complexes	9.65	50,54
X40	NCED	31	Binding energies of non-covalent interactions involving halogenated molecules	5.26	55
A21x12	NCED	252	PECs for the 21 equilibrium complexes from A24	1.43	56
BzDC215	NCED	215	PECs for benzene interacting with two rare-gas atoms and eight first- and second-row hydrides	1.81	57
HW30	NCED	30	Binding energies of hydrocarbon-water dimers	2.34	58
NC15	NCED	15	Binding energies of very small non-covalent complexes	0.95	59
S66	NCED	66	Binding energies of non-covalent interactions found in organic molecules and biomolecules	6.88	60,61
S66x8	NCED	528	PECs for the 66 complexes from S66	5.57	60
3B-69-DIM	NCED	207	Binding energies of all relevant pairs of monomers from 3B-69-TRIM	5.87	62
AlkBind12	NCED	12	Binding energies of saturated and unsaturated hydrocarbon dimers	3.14	63
CO2Nitrogen16	NCED	16	Binding energies of CO_2 to molecular models of pyridinic N-doped graphene	3.84	64
HB49	NCED	49	Binding energies of small- and medium-sized hydrogen-bonded systems	14.12	65–67
Ionic43	NCED	43	Binding energies of anion-neutral, cation-neutral, and anion-cation dimers	69.94	68
H2O6Bind8	NCEC	8	Binding energies of isomers of $(H_2O)_6$	46.96	69,70
HW6Cl	NCEC	6	Binding energies of $Cl^-(H_2O)_n$ ($n = 1-6$)	57.71	69,70
HW6F	NCEC	6	Binding energies of $F^-(H_2O)_n$ ($n = 1-6$)	81.42	69,70
FmH2O10	NCEC	10	Binding energies of isomers of $F^-(H_2O)_{10}$	168.50	69,70
Shields38	NCEC	38	Binding energies of $(H_2O)_n$ ($n = 2-10$)	51.54	71
SW49Bind345	NCEC	31	Binding energies of isomers of $SO_4{}^{2-}(H_2O)_n$ ($n = 3-5$)	28.83	72
SW49Bind6	NCEC	18	Binding energies of isomers of $SO_4{}^{2-}(H_2O)_6$	62.11	72
WATER27	NCEC	23	Binding energies of neutral and charged water clusters	67.48	73,74
3B-69-TRIM	NCEC	69	Binding energies of trimers, with three different orientations of 23 distinct molecular crystals	14.36	62
CE20	NCEC	20	Binding energies of water, ammonia, and hydrogen fluoride clusters	30.21	75,76
H2O20Bind10	NCEC	10	Binding energies of isomers of $(H_2O)_{20}$ (low-energy structures)	198.16	70
H2O20Bind4	NCEC	4	Binding energies of isomers of $(H_2O)_{20}$ (dod, fc, fs, and es)	206.12	73,74,77,78
TA13	NCD	13	Binding energies of dimers involving radicals	22.00	79
XB18	NCD	8	Binding energies of small halogen-bonded dimers	5.23	80
Bauza30	NCD	30	Binding energies of halogen-, chalcogen-, and pnicogen-bonded dimers	23.65	81,82
CT20	NCD	20	Binding energies of charge-transfer complexes	1.07	83
XB51	NCD	20	Binding energies of large halogen-bonded dimers	6.06	80
AlkIsomer11	IE	11	Isomerization energies of $n = 4-8$ alkanes	1.81	84
Butanediol65	IE	65	Isomerization energies of butane-1,4-diol	2.89	85
ACONF	IE	15	Isomerization energies of alkane conformers	2.23	74,86
CYCONF	IE	11	Isomerization energies of cysteine conformers	2.00	74,87
Pentane14	IE	14	Isomerization energies of stationary points on the n-pentane torsional surface	6.53	88
SW49Rel345	IE	31	Isomerization energies of $SO_4{}^{2-}(H_2O)_n$ ($n = 3-5$)	1.47	72
SW49Rel6	IE	18	Isomerization energies of $SO_4{}^{2-}(H_2O)_6$	1.22	72
H2O16Rel5	IE	5	Isomerization energies of $(H_2O)_{16}$ (boat and fused cube structures)	0.40	89
H2O20Rel10	IE	10	Isomerization energies of $(H_2O)_{20}$ (low-energy structures)	2.62	70
H2O20Rel4	IE	4	Isomerization energies of $(H_2O)_{20}$ (dod, fc, fs, and es)	5.68	73,74,77,78
Melatonin52	IE	52	Isomerization energies of melatonin	5.54	90
YMPJ519	IE	519	Isomerization energies of the proteinogenic amino acids	8.33	91
EIE22	ID	22	Isomerization energies of enecarbonyls	4.97	92
Styrene45	ID	45	Isomerization energies of C_8H_8	68.69	93
DIE60	ID	60	Isomerization energies of reactions involving double-bond migration in conjugated dienes	5.06	94
ISOMERIZATION20	ID	20	Isomerization energies	44.05	95
C20C24	ID	8	Isomerization energies of the ground state structures of C_{20} and C_{24}	36.12	96
AlkAtom19	TCE	19	$n = 1-8$ alkane atomization energies	1829.31	84
BDE99nonMR	TCE	83	Bond dissociation energies (SR)	114.98	95
G21EA	TCE	25	Adiabatic electron affinities of atoms and small molecules	40.86	74,97
G21IP	TCE	36	Adiabatic ionization potentials of atoms and small molecules	265.35	74,97
TAE140nonMR	TCE	124	Total atomization energies (SR)	381.05	95
AlkIsod14	TCE	14	$n = 3-8$ alkane isodesmic reaction energies	10.35	84
BH76RC	TCE	30	Reaction energies from HTBH38 and NHTBH38	30.44	74,98,99
EA13	TCE	13	Adiabatic electron affinities	42.51	100
HAT707nonMR	TCE	505	Heavy-atom transfer energies (SR)	74.79	95
IP13	TCE	13	Adiabatic ionization potentials	256.24	100
NBPRC	TCE	12	Reactions involving NH_3/BH_3 and PH_3/BH_3	30.52	74,101,102
SN13	TCE	13	Nucleophilic substitution energies	25.67	95
BSR36	TCE	36	Hydrocarbon bond separation reaction energies	20.06	102,103
HNBrBDE18	TCE	18	Homolytic N–Br bond dissociation energies	56.95	104
WCPT6	TCE	6	Tautomerization energies for water-catalyzed proton-transfer reactions	7.53	105
BDE99MR	TCD	16	Bond dissociation energies (MR)	54.51	95
HAT707MR	TCD	202	Heavy-atom transfer energies (MR)	83.41	95
TAE140MR	TCD	16	Total atomization energies (MR)	147.20	95
PlatonicHD6	TCD	6	Homodesmotic reactions involving platonic hydrocarbon cages, C_nH_n ($n = 4, 6, 8, 10, 12, 20$)	136.71	106
PlatonicID6	TCD	6	Isodesmic reactions involving platonic hydrocarbon cages, C_nH_n ($n = 4, 6, 8, 10, 12, 20$)	96.19	106
PlatonicIG6	TCD	6	Isogyric reactions involving platonic hydrocarbon cages, C_nH_n ($n = 4, 6, 8, 10, 12, 20$)	356.33	106
PlatonicTAE6	TCD	6	Total atomization energies of platonic hydrocarbon cages, C_nH_n ($n = 4, 6, 8, 10, 12, 20$)	2539.27	106
BHPERI26	BH	26	Barrier heights of pericyclic reactions	23.15	74,107
CRBH20	BH	20	Barrier heights for cycloreversion of heterocyclic rings	46.40	108
DBH24	BH	24	Diverse barrier heights	28.34	109,110
CR20	BH	20	Cycloreversion reaction energies	22.31	111
HTBH38	BH	38	Hydrogen transfer barrier heights	16.05	99
NHTBH38	BH	38	Non-hydrogen transfer barrier heights	33.48	98
PX13	BH	13	Barrier heights for proton exchange in water, ammonia, and hydrogen fluoride clusters	28.83	75,76
WCPT27	BH	27	Barrier heights of water-catalyzed proton-transfer reactions	38.73	105
AE18	–	18	Absolute atomic energies of hydrogen through argon	148,739.00	112
RG10	–	569	PECs for the 10 rare-gas dimers involving helium through krypton	1.21	113

marked.

The NCED category is comprised of 1744 "easy" (i.e. not significantly affected by SC or SIE) binding energies of non-covalent dimers, including both equilibrium and non-equilibrium separations. M06-2X is the best performer, with an overall root-mean-square-deviation (RMSD) of 0.43 kcal/mol, followed by MN15 (0.47 kcal/mol). M06-L, M08-SO, and M08-HX, with RMSDs of 0.55, 0.56, and 0.58 kcal/mol, respectively, perform between 15% and 35% worse than the two best Minnesota functionals. M11, M05-2X, M06, and M06-HF have RMSDs between 0.65 and 0.85 kcal/mol, while the remaining five functionals perform very poorly. MN12-SX, MN12-L, and M11-L have RMSDs of about 1 kcal/mol, while MN15-L has the second-largest RMSD of 1.38 kcal/mol. However, the worst overall performance is attributed to M05 (1.53 kcal/mol). Interestingly, the newer local Minnesota functionals (M11-L, MN12-L, and MN15-L) perform between 2 and 3 times worse than their decade-old predecessor, M06-L.

The NCEC category is comprised of 243 binding energies of non-covalent clusters including water, halide-water, and sulfate-water clusters. Due to the greater magnitude of these interactions, the RMSDs for this category are naturally larger than those from the previous category. The functional that performs best for the conventional closed-shell non-covalent dimers (M06-2X) tends to overbind these clusters and affords an RMSD of 2.52 kcal/mol. The best hybrid functionals are M08-HX, MN15, and M08-SO, with RMSDs of 1.73, 1.83 and 2.14 kcal/mol, respectively, while the best local functional is, by far, M06-L (2.20 kcal/mol). The other three local Minnesota functionals, M11-L, MN12-L, and MN15-L, perform successively worse and strongly underbind these clusters, with very large RMSDs of 9.47, 11.65, and 12.83 kcal/mol, respectively. While M05 performs nearly 60% worse than M05-2X (2.44 kcal/mol), M06 and M11 perform only about 15% worse than M06-2X. Finally, the remaining hybrid functionals, M06-HF and MN12-SX, perform very poorly for these clusters, with the former overbinding the clusters and affording an RMSD of 4.97 kcal/mol, and the latter underbinding them with an RMSD of 8.61 kcal/mol. As with the previous category, the newer local Minnesota functionals (M11-L, MN12-L, and MN15-L) perform between 4 and 6 times worse than M06-L.

The NCD category contains 91 non-covalent dimer binding energies that are highly susceptible to self-interaction error. As a result, functionals with high percentages of exact exchange should perform better than their counterparts. Accordingly, the four best functionals are M08-SO (56.79%), MN15 (44%), M06-2X (54%), and M08-HX (52.23%), all with RMSDs around 1 kcal/mol. Contrary to this trend, however, M06-HF performs worst out of all of the functionals considered, with an RMSD of 1.95 kcal/mol, and M05-2X (1.55 kcal/mol) performs more than 50% worse than M06-2X, albeit having slightly more exact exchange. M11, with 42.8% short-range exact exchange, performs reasonably well, with an RMSD of 1.23 kcal/mol, while the rest of the hybrids (M06, M05, and MN12-SX) have RMSDs around 1.55 kcal/mol. The best local functional is MN12-L (1.29 kcal/mol), followed by MN15-L (1.45 kcal/mol) and M11-L (1.65 kcal/mol), with M06-L performing most poorly (1.87 kcal/mol). Thus, MN12-L and MN15-L surprisingly outperform all of the hybrid functionals except M08-SO, MN15, M06-2X, M08-HX, and M11.

The next category, IE, contains 755 isomerization energies of organic compounds, water clusters, and sulfate-water clusters. The best functional for these relative energies, by a considerable margin, is M05-2X, with an RMSD of 0.41 kcal/mol. The next best functional is M06-2X, with an RMSD (0.50 kcal/mol) that is more than 20% worse than that of M05-2X. M05-2X and M06-2X are followed by three other hybrids, M08-HX, MN12-SX, and M06-HF, which have RMSDs around 0.6 kcal/mol. From the local functionals, M11-L and M06-L perform very similarly, with RMSDs of 0.69 and 0.71 kcal/mol, respectively, while the two newest local Minnesota functionals perform considerably worse, with MN12-L affording an RMSD of 1.06 kcal/mol and MN15-L affording the worst overall RMSD of 1.55 kcal/mol. From the five re-

maining hybrid functionals, M05 performs the worst, with an RMSD of 1.13 kcal/mol, while the other four (MN15, M08-SO, M11, and M06) perform similarly with RMSDs around 0.75 kcal/mol.

The ID category contains 155 isomerization energies that are highly susceptible to self-interaction error. As with the NCD category, functionals with a high percentage of exact exchange should be competitive for these interactions. Accordingly, the seven best functionals are the seven hybrid Minnesota functionals with at least 40% exact exchange, with M08-SO and MN15 having RMSDs around 4 kcal/mol, M08-HX and M05-2X having RMSDs around 4.65 kcal/mol, and M06-2X, M11, and M06-HF having RMSDs between 5.5 and 6 kcal/mol. From the local functionals, M11-L has the smallest RMSD of 5.99 kcal/mol, followed by MN15-L and MN12-L, which have RMSDs of 6.94 and 7.93 kcal/mol, respectively. M06-L is the worst-performing functional overall, with an RMSD of 10.16 kcal/mol, while the three hybrids with the largest RMSDs are MN12-SX, M06, and M05, with RMSDs of 6.37, 8.17, and 8.67 kcal/mol, respectively.

The TCE category contains 947 data points including atomization energies, bond dissociation energies, electron affinities, ionization potentials, and various reaction energies. M06-2X, with an RMSD of 3.29 kcal/mol, is the best functional for this category by a comfortable margin. The next best functionals, M08-HX and M11, are both hybrids and perform about 10% worse than M06-2X, while MN15 (3.76 kcal/mol) performs about 15% worse than M06-2X. Among the remaining hybrid functionals, MN12-SX, M05, and M06-HF perform much more poorly, with RMSDs of 5.46, 5.48, and 5.82 kcal/mol, respectively, while M05-2X, M08-SO, and M06 have RMSDs around 4 kcal/mol. Among the local functionals, MN15-L, with an RMSD of 4.62 kcal/mol, ranks first, followed by MN12-L (4.95 kcal/mol) and M06-L (5.44 kcal/mol). M11-L is the worst-performing functional for these conventional bonded interactions, with a very large RMSD of 7.22 kcal/mol.

The TCD category contains the 234 multi-reference data points from the W4-11 dataset, as well as 24 atomization energies and homodesmotic, isodesmic, and isogyric reactions from the Platonic24 dataset. While the first grouping should be a major challenge for hybrid functionals due to SC, the second grouping should present difficulties for local functionals due to SIE. With an RMSD of 6.44 kcal/mol, MN15 is the best overall performer, followed by two hybrids (M06-2X and M06 with RMSDs of about 7.25 kcal/mol) and surprisingly, a local functional (MN12-L with an RMSD of 7.47 kcal/mol). The 2008 functionals perform similarly, with RMSDs around 8.1 kcal/mol, followed by M05-2X and MN15-L, with RMSDs of 8.49 and 8.62 kcal/mol, respectively. The remaining six functionals have RMSDs in excess of 9 kcal/mol, with the two worst performers being M06-L (12.97 kcal/mol) and M06-HF (14.08 kcal/mol).

The BH category contains 206 barrier heights, some of which come from datasets that the Minnesota functionals were trained on, and some of which come from recent benchmarks carried out by Karton and coworkers. M06-2X, with an RMSD of 2.57 kcal/mol, is significantly outperformed by three of the newer hybrid Minnesota density functionals: M08-SO (1.78 kcal/mol), M08-HX (1.80 kcal/mol), and MN15 (1.98 kcal/mol). The impressive accuracy of the 2008 Minnesota functionals for barrier heights has been previously demonstrated by Truhlar and coworkers,[114–118] while the positive result for MN15 is quite encouraging. Three other hybrid functionals (M11, MN12-SX, and M05-2X) perform between 10% and 30% worse than M06-2X, with RMSDs between 2.8 and 3.5 kcal/mol. The remaining three hybrids (M06, M05, and M06-HF) perform very poorly, with RMSDs in excess of 5 kcal/mol. Local functionals conventionally tend to perform rather poorly for barrier heights, but the best-performing local functionals, MN12-L and MN15-L, with RMSDs of 4.29 and 4.78 kcal/mol, respectively, outperform the three poorest hybrids. M11-L (5.39 kcal/mol) and M06-L (6.85 kcal/mol) perform significantly more poorly. As expected, the best-performing local functionals are unable to come close to the performance of the best hy-

brids.

4.2 Results for Selected Datasets

Since assessing the performance of the Minnesota density functionals on each of the 84 datasets would be an arduous task, at least one and at most two representative datasets will be selected from each datatype and discussed. The complete set of results for all datasets is summarized in four tables: non-covalent interactions (Table 4), isomerization energies (Table 5), thermochemistry (Table 6), and barrier heights (Table 7).

The S22 dataset has served as a trustworthy benchmark for assessing the accuracy of a wide variety of methods for non-covalent interactions in the past decade and will therefore be used as a representative from the NCED category. Consistent with the overall statistics from Section 4.1, M06-2X performs best with an RMSD of 0.54 kcal/mol, while M06 performs more than 2 times worse with an RMSD of 1.20 kcal/mol. M06-L, with an RMSD of 0.83 kcal/mol, is the best local functional, as its newer counterparts perform much more poorly, with large RMSDs of 1.48 kcal/mol (MN12-L), 1.68 kcal/mol (M11-L), and 2.52 kcal/mol (MN15-L). The 2005 Minnesota density functionals both perform poorly, with M05-2X having an RMSD slightly larger than 1 kcal/mol, and M05 having the largest RMSD (2.88 kcal/mol) out of all of the functionals. MN12-SX performs much worse than M11, with an RMSD of 1.55 kcal/mol compared to 0.88 kcal/mol, while M08-HX performs 20% better than M08-SO (0.81 kcal/mol). Surprisingly, M06-HF ranks third among the Minnesota functionals for this dataset, with an RMSD of 0.79 kcal/mol. Finally, despite being partially trained on the S66x8 dataset, the performance of MN15 for the S22 dataset is disappointing, as it ranks sixth among the 14 benchmarked functionals, with an RMSD of 0.84 kcal/mol. Furthermore, MN15, with an RMSD of 0.64 kcal/mol, is only sixth best for the S66 dataset itself, while M06-2X performs nearly 2 times better with an RMSD of 0.33 kcal/mol.

Since the S22 dataset contains a mixture of hydrogen-bonded and dispersion-bound systems, it is useful to consider an additional dataset that deals specifically with the latter. For this purpose, the AlkBind12 dataset, which contains saturated and unsaturated hydrocarbon dimers, will be analyzed. The RMS of the 12 reference energies comprising AlkBind12 is only 3.14 kcal/mol, indicating that the systems are weakly bound. The three best functionals, M08-SO, M08-HX, and M06-2X, have RMSDs between 0.25 and 0.3 kcal/mol, while the best local functional is M06-L, with an RMSD of 0.38 kcal/mol. These RMSDs represent an error on the order of 10%, which is quite reasonable. On the other hand, MN15-L, with a very large RMSD of 3.49 kcal/mol, drastically overbinds these systems. The only other functional that manages to overbind these dimers is MN15, which has an RMSD (1.18 kcal/mol) that is 4 times larger than that of M06-2X. Thus, the two newest Minnesota functionals show a tendency to greatly overbind these dispersion interactions. Of the remaining functionals, M05-2X, MN12-SX, M06-HF, and M05 perform poorly as well, with RMSDs in excess of 1 kcal/mol (due to underbinding), while M06, M11, MN12-L, and M11-L have RMSDs of 0.49, 0.51, 0.56, and 0.79 kcal/mol, respectively.

In order to assess the performance of the Minnesota functionals for non-covalent clusters (NCEC), the H2O20Bind10 dataset, which contains 10 water 20-mer isomer binding energies, will be selected for analysis. Contrary to the overall results from Section 4.1, M05-2X (3.07 kcal/mol) and M06-2X (3.50 kcal/mol) have the smallest RMSDs for this dataset, while M08-HX and MN15 place third and fifth, with RMSDs of 3.91 and 6.74 kcal/mol, respectively. Furthermore, while M05-2X and M06-2X both overbind the clusters, M08-HX and MN15 underbind them. The best local functional, by far, is M06-L, with an RMSD of 6.32 kcal/mol, while the newer local functionals have RMSDs that are 4 to 8 times larger, with MN15-L affording the largest overall RMSD of 46.44 kcal/mol. Additionally, all four of the local functionals underbind the clusters. Five of the six remaining hybrids (M08-SO, M06, M11,

Table 3: RMSDs in kcal/mol for 8 datatypes for the 14 Minnesota density functionals. NCED stands for non-covalent dimers (easy), NCEC stands for non-covalent clusters (easy), NCD stands for non-covalent dimers (difficult), IE stands for isomerization energies (easy), ID stands for isomerization energies (difficult), TCE stands for thermochemistry (easy), TCD stands for thermochemistry (difficult), and BH stands for barrier heights. The partitioning of the 4399 data points contained in this table into the 8 datatypes is: 1744, 243, 91, 755, 155, 947, 258, and 206.

Datatype	M05	M05-2X	M06	M06-2X	M06-HF	M08-HX	M08-SO	M11	MN12-SX	MN15	M06-L	M11-L	MN12-L	MN15-L
NCED	1.53	0.67	0.71	0.43	0.82	0.58	0.56	0.65	0.99	0.47	0.55	1.18	1.08	1.38
NCEC	3.85	2.44	2.88	2.52	4.97	1.73	2.14	2.82	8.61	1.83	2.20	9.47	11.65	12.83
NCD	1.55	1.55	1.54	0.99	1.95	1.03	0.91	1.23	1.57	0.96	1.87	1.65	1.29	1.45
IE	1.13	0.41	0.77	0.50	0.61	0.59	0.71	0.74	0.61	0.71	0.71	0.69	1.06	1.55
ID	8.67	4.66	8.17	5.56	5.89	4.62	3.95	5.65	6.37	4.06	10.16	5.99	7.93	6.94
TCE	5.48	3.98	4.11	3.29	5.82	3.60	4.03	3.67	5.46	3.76	5.44	7.22	4.95	4.62
TCD	9.59	8.49	7.27	7.23	14.08	8.14	8.12	9.19	10.26	6.44	12.97	11.09	7.47	8.62
BH	5.83	3.41	5.05	2.57	6.48	1.80	1.78	2.82	3.05	1.98	6.85	5.39	4.29	4.78

M05, and M06-HF) have RMSDs between 7 and 13 kcal/mol, with the first four underbinding the clusters, and M06-HF overbinding them. The worst hybrid functional, MN12-SX, comes in with an (underbound) RMSD of 30.40 kcal/mol, performing more than 3 times worse than its range-separated counterpart, M11.

Representing the NCD category, the TA13 dataset contains 13 interactions involving radicals, most of which are heavily prone to self-interaction error. Functionals with large fractions of exact exchange should generally perform well for these types of systems, and it is not surprising that the four best functionals (M06-2X, M06-HF, M08-HX, and M08-SO), with RMSDs ranging from 1.38 to 1.77 kcal/mol, have at least 50% exact exchange. The best-performing local functional is MN15-L (1.77 kcal/mol), which surprisingly matches the performance of M08-SO, slightly outperforms M11 (1.82 kcal/mol), and is not very far behind M06-2X (1.38 kcal/mol). While MN12-L (1.86 kcal/mol) performs only slightly worse than MN15-L, M11-L (2.65 kcal/mol) and M06-L (3.78 kcal/mol) yield significantly larger RMSDs. The hybrids with less than 50% exact exchange, namely MN15, M06, M05, and MN12-SX, have RMSDs of 2.12, 2.35, 2.92, and 3.28 kcal/mol, respectively. From the hybrid functionals, the outlier is M05-2X, which has an RMSD of 2.54 kcal/mol, despite having 56% exact exchange.

An example from the IE category, the Butanediol65 dataset contains the relative energies of 65 isomers of butane-1,4-diol. The best performing functionals for this dataset, with RMSDs between 0.15 and 0.25 kcal/mol, are the four density functionals from 2006, with M06 (0.16 kcal/mol) only slightly outperforming M06-HF, M06-2X, and M06-L. In contrast to the impressive performance of M06-L (0.23 kcal/mol), the newer local functionals, M11-L, MN12-L and MN15-L, perform successively more poorly with RMSDs that are 2.75, 3.5, and 5 times larger, respectively. M05-2X and the two functionals from 2008 perform similarly, with RMSDs around 0.3 kcal/mol, while M11 performs slightly worse but still almost 2 times better than MN12-SX (0.70 kcal/mol). While M06 is the best density functional for the Butanediol65 dataset, its older and newer cousins, M05 and MN15, perform almost 3 times worse (0.44 and 0.47 kcal/mol, respectively), with MN15 being the worst-performing global hybrid.

Since the Butanediol65 dataset deals specifically with the isomerization energies of a small organic compound, the H2O16Rel5 dataset will be used to assess the performance of the Minnesota functionals for predicting the relative energies of the five lowest-energy structures of $(H_2O)_{16}$. According to the CCSD(T) calculations performed by Xantheas and coworkers, the most stable isomer is 4444-a, followed

by the boat-a, boat-b, antiboat, and 4444-b isomers, which are 0.255, 0.421, 0.511, and 0.542 kcal/mol less stable than the 4444-a isomer, respectively. Thus, the RMS of the H2O16Rel5 reference energies is approximately 0.4 kcal/mol. Only two of the Minnesota functionals (M06-HF and M05-2X) manage RMSDs that are around 0.4 kcal/mol. The worst-performing functional, MN15-L, has an RMSD of 5.03 kcal/mol, because it erroneously predicts the three boat isomers to be nearly 7 kcal/mol higher in energy than the most stable fused-cube structure. In addition, M06-L, MN12-L, and M06 perform very poorly, with RMSDs in excess of 2 kcal/mol. The rest of the functionals have RMSDs that lie between 1 and 2 kcal/mol.

The DIE60 dataset from ID contains 60 diene isomerization energies that are susceptible to delocalization error. Not surprisingly, the four local functionals perform the worst, with RMSDs between 2 and 3 kcal/mol. Contrary to expectation, however, M06-HF performs rather poorly, with an RMSD of 1.54 kcal/mol. Besides M06-HF, the three worst hybrids, M06, MN12-SX, and M05, all have less than 30% exact exchange, and RMSDs between 1.4 and 1.75 kcal/mol. The six remaining hybrid functionals, M05-2X, M06-2X, M08-SO, M08-HX, MN15, and M11, have at least 40% exact exchange and perform well, with RMSDs below 1 kcal/mol. M05-2X performs the best, with an RMSD of 0.61 kcal/mol, followed by M06-2X and M08-SO, with RMSDs around 0.85 kcal/mol, while the latter three functionals have RMSDs around 1 kcal/mol.

The TAE140 dataset from the W4-11 database contains 140 total atomization energies of small molecules. Since 16 of these molecules have multi-reference character, the TAE140nonMR subset of 124 molecules will be used as the representative dataset for TCE. The two best Minnesota functionals are M08-HX and M06-2X, with small RMSDs of 2.88 and 2.98 kcal/mol, respectively, followed by MN15 (3.15 kcal/mol). While M08-HX performs the best, its second-order-constrained counterpart, M08-SO, is more than 30% worse, with an RMSD of 3.85 kcal/mol. M06, M11, and M05 have similar RMSDs ranging from 3.6 to 3.8 kcal/mol, while M05-2X has an RMSD slightly over 4 kcal/mol. MN15-L, with an RMSD of 4.30 kcal/mol, is the best local functional, followed by MN12-L (4.66 kcal/mol) and M06-L (5.43 kcal/mol). While MN12-L is less than 10% worse than MN15-L, M11-L, with an RMSD of 7.94 kcal/mol, performs about 85% worse than MN15-L, and has the largest RMSD among the 14 functionals. The worst-performing hybrid functionals are MN12-SX and M06-HF, with RMSDs in excess of 5.5 kcal/mol.

Since all of the Minnesota density functionals have been trained on the atomization energies of small molecules, it is useful to assess their transferability to the atomization energies of larger systems. For this purpose, the AlkAtom19 dataset, which contains 19 atomization energies of linear and branched alkanes (methane through octane), will be utilized. The RMSDs for this dataset range from 3.78 kcal/mol (M05-2X) to 30.82 kcal/mol (M11-L). Surprisingly, the top three functionals for TAE140nonMR (M08-HX, M06-2X, and MN15) rank fifth, seventh, and eleventh for AlkAtom19, with RMSDs of 7.38, 8.02, and 14.67 kcal/mol, respectively. After M05-2X, the three best-performing hybrid functionals are M06, M05, and M11, with RMSDs between 4.5 and 5.5 kcal/mol. While MN12-L and MN15-L outperform M06-L for the TAE140nonMR dataset, the reverse is true for AlkAtom19, with M06-L (9.63 kcal/mol) performing nearly 20% better than MN12-L (11.65 kcal/mol) and more than 40% better than MN15-L (17.04 kcal/mol). Of the three remaining hybrids, M06-HF has an RMSD of 7.73 kcal/mol, M08-SO performs nearly 40% worse than M08-HX, while MN12-SX (25.71 kcal/mol) performs almost 5 times worse than M11.

Although the multi-reference systems in TCD lie outside the scope of most existing Kohn-Sham density functionals, it is nevertheless interesting to discuss the performance of the Minnesota functionals on the 16 multi-reference molecules from TAE140. The RMSDs for TAE140MR lie between 4 and 20 kcal/mol, with MN15-L exhibiting the best performance

(4.48 kcal/mol) and M06-HF exhibiting the worst performance (19.43 kcal/mol). The only other local functional that comes at all close to MN15-L is M06-L, with an RMSD of 6.30 kcal/mol. The other two local functionals, MN12-L and M11-L, perform 45% and 70% worse than M06-L, respectively. From the hybrid functionals, M06 performs the best, with an RMSD of 5.32 kcal/mol. Only two other hybrids perform comparably to M06: MN15, with an RMSD of 5.63 kcal/mol, and M05, with an RMSD of 6.16 kcal/mol. The rest of the hybrid functionals (M11, M06-2X, MN12-SX, M08-HX, M08-SO, and M05-2X) have RMSDs that lie between 7.7 kcal/mol and 10.3 kcal/mol.

From the BH category, the recent CRBH20 dataset which contains 20 cycloreversion barrier heights of heterocyclic rings will be analyzed. MN15, M11, and M08-HX, the three functionals with the best performance, have RMSDs under 1.3 kcal/mol, while M06-2X comes in fourth with an RMSD of 1.58 kcal/mol. Not surprisingly, the two worst functionals, M11-L and M06-L, are both local and have RMSDs of 9.70 and 13.73 kcal/mol, respectively. By contrast, the best local functionals are MN12-L and MN15-L, with RMSDs of 6.55 and 7.18 kcal/mol, respectively. The only other hybrid functional that performs reasonably well is M08-SO, with an RMSD of 1.80 kcal/mol. The RMSDs for the rest of the hybrids range from 2.75 to 10 kcal/mol, with M05 (7.84 kcal/mol), M06 (8.74 kcal/mol), and M06-HF (9.56 kcal/mol) exhibiting the worst performance. While the performance of M05-2X is not great (2.77 kcal/mol), it is almost 3 times better than that of M05, while the performance of MN12-SX (3.97 kcal/mol) is 3 times worse than that of M11.

4.3 Potential Energy Curves

The BzDC215, NBC10, and S66x8 datasets contain potential energies curves (PEC) that can be used to assess the accuracy of density functionals for predicting equilibrium properties of dimers. Furthermore, the RG10 dataset contains all 10 PECs that can be constructed between the rare-gas dimers from helium to krypton. In total, these 4 datasets contain 96 PECs, with BzDC215, NBC10, and RG10 each having 10, and S66x8 having 66. Unfortunately, even with the use of fine grids, some of the resulting potential energy curves are too oscillatory to be accurately interpolated.[119–121] Consequently, the benzene-neon dimer and the benzene-argon dimer PECs from BzDC215 were removed, the sandwich benzene dimer, the methane dimer, and the sandwich (S2) pyridine dimer PECs from NBC10 were removed, and the helium dimer PEC from RG10 was removed, leaving a total of 90 potential energy curves.

Table 8 contains the equilibrium bond length (EBL) and equilibrium binding energy (EBE) RMSDs for these 4 datasets, along with the corresponding total RMSDs with RG10 excluded (All*). A noticeable trend is that functionals that are able to predict accurate equilibrium bond lengths perform much worse for the equilibrium binding energies, and vice-versa. This is not a desired attribute of a density functional and is a disadvantage of using the Minnesota functionals for describing non-covalent interactions. In order to keep the discussion succinct, only the RG10 and All* results will be discussed.

The performance of most of the Minnesota functionals for rare-gas dimers has been previously shown to be relatively very poor.[122–124] Indeed, 12 of the 14 functionals have EBL RMSDs larger than 0.1 Å. MN15-L and MN15 perform well for the rare-gas dimers, primarily because their training set includes a handful of data points from several rare-gas dimer PECs. Besides these two functionals, only M05-2X does not have a very poor result for the RG10 EBL, managing an RMSD of 0.137 Å. The rest of the functionals have RMSDs larger than 0.2 Å, and the three worst functionals, by far, are MN12-SX, MN12-L, and M11-L, which have RMSDs in excess of 1 Å. Figure 1 shows the krypton dimer PEC as determined by all 14 functionals, and it is clear that the PECs for MN12-SX, MN12-L, and M11-L are completely unphysical. For these three functionals, it is difficult to decide where the minimum lies, since the PECs either have a saddle point (MN12-SX

Table 4: RMSDs in kcal/mol for 36 non-covalent interaction datasets for the 14 Minnesota density functionals. NCED stands for non-covalent dimers (easy), NCEC stands for non-covalent clusters (easy), and NCD stands for non-covalent dimers (difficult). Table 2 contains specific information regarding the datasets, and the datatypes are explained in Section 3.

Dataset	Datatype	M05	M05-2X	M06	M06-2X	M06-HF	M08-HX	M08-SO	M11	MN12-SX	MN15	M06-L	M11-L	MN12-L	MN15-L
A24	NCED	0.28	0.28	0.35	0.26	0.42	0.22	0.23	0.35	0.50	0.31	0.35	0.77	0.72	0.57
DS14	NCED	0.86	0.37	0.53	0.25	0.50	0.18	0.20	0.55	0.86	0.25	0.43	0.98	0.95	0.69
HB15	NCED	0.74	0.45	0.67	0.36	0.76	0.45	0.87	0.54	1.33	0.66	0.58	1.61	1.62	2.32
HSG	NCED	1.23	0.62	0.74	0.52	0.90	0.68	0.58	0.88	1.18	0.28	0.63	1.39	1.46	0.83
NBC10	NCED	2.42	1.12	0.86	0.56	0.78	0.69	0.56	0.87	0.97	0.34	0.61	0.92	0.95	1.25
S22	NCED	2.88	1.05	1.20	0.54	0.79	0.64	0.81	0.88	1.55	0.84	0.83	1.68	1.48	2.52
X40	NCED	1.28	0.59	0.76	0.32	0.66	0.50	0.44	0.74	1.07	0.36	0.59	1.42	1.23	1.18
A21x12	NCED	0.16	0.15	0.20	0.14	0.22	0.18	0.19	0.18	0.34	0.19	0.22	0.54	0.46	0.40
BzDC215	NCED	1.05	0.34	0.47	0.34	0.78	0.49	0.53	0.31	0.45	0.53	0.34	0.60	0.42	0.77
HW30	NCED	0.36	0.32	0.46	0.37	0.55	0.34	0.34	0.36	0.53	0.44	0.51	0.88	0.72	0.56
NC15	NCED	0.17	0.12	0.28	0.14	0.23	0.15	0.13	0.22	0.35	0.12	0.26	0.69	0.48	0.09
S66	NCED	1.87	0.70	0.80	0.33	0.77	0.38	0.44	0.61	1.20	0.64	0.61	1.34	1.15	2.16
S66x8	NCED	1.76	0.61	0.74	0.38	0.67	0.58	0.53	0.57	1.09	0.48	0.52	1.28	1.14	1.60
3B-69-DIM	NCED	1.24	0.64	0.95	0.52	0.67	0.74	0.72	0.87	1.29	0.48	0.72	1.57	1.49	1.27
AlkBind12	NCED	2.25	0.99	0.49	0.30	1.44	0.28	0.25	0.51	1.02	1.18	0.38	0.79	0.56	3.49
CO2Nitrogen16	NCED	1.85	0.70	1.44	0.36	0.34	0.58	0.57	0.86	1.39	0.36	1.16	2.16	1.54	0.82
HB49	NCED	0.90	0.65	0.75	0.56	1.10	0.48	0.63	0.63	1.37	0.58	0.72	2.05	1.81	2.00
Ionic43	NCED	1.85	1.71	0.78	1.16	3.06	1.38	1.36	1.63	1.50	0.73	1.02	1.50	1.71	2.39
H2O6Bind8	NCEC	0.90	1.89	1.64	1.60	3.89	0.65	0.81	0.97	5.52	0.45	1.35	6.62	7.43	10.01
HW6Cl	NCEC	1.78	2.46	0.93	2.84	3.72	2.31	2.16	0.93	3.88	2.08	0.90	5.20	4.29	5.18
HW6F	NCEC	1.74	4.01	0.97	4.07	6.13	2.02	1.78	1.69	3.17	2.33	1.23	3.04	4.20	5.83
FmH2O10	NCEC	6.52	7.29	2.67	8.53	12.08	3.01	2.63	1.73	11.73	3.47	3.33	10.38	13.54	17.61
Shields38	NCEC	1.70	1.96	1.90	1.77	4.25	0.51	0.60	1.19	6.44	0.63	1.47	8.89	9.31	10.44
SW49Bind345	NCEC	1.69	0.07	0.40	0.57	0.96	0.60	0.64	0.88	2.20	0.19	0.42	2.42	2.31	2.15
SW49Bind6	NCEC	3.40	0.17	0.57	0.90	1.17	1.15	0.93	1.88	4.88	0.49	0.44	5.32	5.34	5.11
WATER27	NCEC	2.04	2.91	1.92	2.73	6.20	1.26	1.58	1.14	4.85	1.19	1.43	7.19	7.24	8.49
3B-69-TRIM	NCEC	3.27	1.61	2.34	1.31	1.60	1.90	1.80	2.14	3.32	1.11	1.71	3.84	3.69	2.70
CE20	NCEC	1.17	2.01	1.57	1.44	3.23	0.45	0.54	1.70	4.19	1.06	1.34	6.02	5.83	6.32
H2O20Bind10	NCEC	12.15	3.07	8.49	3.50	12.85	3.91	7.46	9.86	30.40	6.74	6.32	28.32	41.10	46.44
H2O20Bind4	NCEC	9.82	4.00	11.52	3.30	10.71	4.75	5.05	9.44	28.29	2.24	8.10	37.11	41.16	40.25
TA13	NCD	2.92	2.54	2.35	1.38	1.60	1.65	1.77	1.82	3.28	2.12	3.78	2.65	1.86	1.77
XB18	NCD	0.53	0.59	0.39	0.58	1.38	0.79	0.27	1.21	1.36	0.28	0.39	1.28	1.10	0.75
Bauza30	NCD	1.73	2.02	2.05	1.30	3.01	1.14	0.90	1.10	0.84	0.81	1.95	1.53	1.31	2.07
CT20	NCD	0.16	0.17	0.68	0.23	0.49	0.35	0.36	0.52	0.83	0.19	0.40	1.32	1.02	0.33
XB51	NCD	0.87	0.63	0.59	0.69	1.06	0.85	0.60	1.43	1.33	0.52	0.89	1.37	1.09	0.89
RG10	-	0.21	0.18	0.23	0.22	0.20	0.23	0.19	0.18	0.23	0.14	0.19	0.38	0.31	0.13

Table 5: RMSDs in kcal/mol for 17 isomerization energy datasets for the 14 Minnesota density functionals. IE stands for isomerization energies (easy) and ID stands for isomerization energies (difficult). Table 2 contains specific information regarding the datasets, and the datatypes are explained in Section 3.

Dataset	Datatype	M05	M05-2X	M06	M06-2X	M06-HF	M08-HX	M08-SO	M11	MN12-SX	MN15	M06-L	M11-L	MN12-L	MN15-L
AlkIsomer11	IE	3.65	0.16	0.27	0.18	0.47	0.34	0.50	0.54	0.78	0.78	0.88	0.90	0.90	1.84
Butanediol65	IE	0.44	0.30	0.16	0.19	0.18	0.33	0.32	0.37	0.70	0.47	0.23	0.64	0.81	1.18
ACONF	IE	0.79	0.11	0.36	0.29	0.14	0.46	0.56	0.73	0.06	0.59	0.49	0.24	0.73	0.85
CYCONF	IE	0.49	0.09	0.15	0.24	0.30	0.33	0.32	0.40	0.29	0.46	0.40	0.53	0.49	0.56
Pentane14	IE	0.42	0.24	0.20	0.13	0.25	0.29	0.48	0.49	0.11	0.32	0.38	0.25	0.30	0.43
SW49Rel345	IE	0.16	0.08	0.43	0.24	0.86	0.32	0.53	0.31	0.29	0.18	0.43	0.27	0.38	0.66
SW49Rel6	IE	0.18	0.12	0.72	0.33	1.03	0.26	0.38	0.24	0.49	0.33	0.73	0.16	0.79	0.98
H2O16Rel5	IE	0.96	0.41	3.82	1.91	0.39	1.08	1.93	1.43	1.47	1.14	2.21	1.19	2.85	5.03
H2O20Rel10	IE	0.61	0.48	2.27	1.44	0.67	0.94	1.16	1.07	0.91	0.91	1.33	0.77	2.08	2.43
H2O20Rel4	IE	1.10	0.53	4.29	1.92	0.37	0.93	1.94	1.24	1.87	1.13	3.01	3.00	2.69	5.92
Melatonin52	IE	2.06	0.41	0.49	0.27	0.43	0.47	0.41	0.74	0.63	0.48	0.88	0.83	1.08	1.55
YMPJ519	IE	1.03	0.45	0.64	0.49	0.65	0.64	0.75	0.80	0.59	0.77	0.65	0.66	1.07	1.51
EIE22	ID	1.30	0.46	1.34	0.37	1.82	0.51	0.32	0.54	1.36	0.86	2.65	1.93	2.50	2.07
Styrene45	ID	9.75	4.56	5.12	2.98	3.70	2.38	2.57	3.62	2.75	3.28	5.79	3.26	3.99	4.55
DIE60	ID	1.71	0.61	1.41	0.84	1.54	0.96	0.87	0.97	1.64	0.97	2.63	2.14	2.36	2.08
ISOMERIZATION20	ID	3.11	1.85	2.44	1.50	4.21	1.78	1.93	2.24	2.77	1.92	3.87	4.56	3.53	2.93
C20C24	ID	29.52	17.07	33.32	23.20	22.87	19.12	15.80	22.90	26.45	15.52	41.27	23.20	32.23	27.43

Table 6: RMSDs in kcal/mol for 23 thermochemistry datasets for the 14 Minnesota density functionals. TCE stands for thermochemistry (easy) and TCD stands for thermochemistry (difficult). Table 2 contains specific information regarding the datasets, and the datatypes are explained in Section 3.

Dataset	Datatype	M05	M05-2X	M06	M06-2X	M06-HF	M08-HX	M08-SO	M11	MN12-SX	MN15	M06-L	M11-L	MN12-L	MN15-L
AlkAtom19	TCE	5.36	3.78	4.53	8.02	7.73	7.38	10.18	5.42	25.71	14.67	9.63	30.82	11.65	17.04
BDE99nonMR	TCE	4.97	3.34	3.64	2.77	6.52	3.52	3.89	3.76	3.06	3.23	5.66	4.94	3.83	3.81
G21EA	TCE	4.72	2.91	3.69	2.81	4.41	2.77	3.14	2.10	3.63	1.94	5.15	5.31	4.79	2.90
G21IP	TCE	4.23	4.39	3.86	3.57	7.55	4.59	4.88	4.85	5.01	3.46	5.45	4.85	5.52	4.25
TAE140nonMR	TCE	3.76	4.05	3.62	2.98	6.48	2.88	3.85	3.74	5.59	3.15	5.43	7.94	4.66	4.30
AlkIsod14	TCE	5.55	1.39	1.84	1.72	0.65	1.93	2.28	2.14	3.11	1.22	3.93	2.47	2.36	0.83
BH76RC	TCE	3.48	1.73	2.45	1.20	3.47	1.55	1.33	2.10	1.96	2.11	4.18	4.31	3.19	3.26
EA13	TCE	4.74	2.25	3.37	2.51	3.04	1.53	2.33	0.75	4.04	1.90	5.10	5.11	5.00	3.09
HAT707nonMR	TCE	5.38	4.45	4.58	3.27	6.04	3.80	4.00	3.80	3.96	3.46	5.36	5.91	5.11	4.17
IP13	TCE	3.27	4.01	3.14	3.18	5.01	4.10	4.57	5.45	3.92	3.33	2.71	3.20	2.76	2.36
NBPRC	TCE	5.62	1.87	3.39	1.28	3.41	2.13	2.61	3.37	2.95	2.32	4.72	5.81	3.25	3.08
SN13	TCE	2.21	1.35	1.83	0.91	2.29	0.90	0.86	1.83	0.84	3.02	1.58	3.62	2.04	2.64
BSR36	TCE	12.26	2.65	3.67	4.46	1.75	3.50	4.00	2.46	5.21	0.61	7.00	3.22	1.50	3.63
HNBrBDE18	TCE	8.14	2.54	3.14	3.07	2.21	0.95	0.85	1.79	2.28	2.50	5.21	3.45	6.32	4.19
WCPT6	TCE	2.15	1.35	1.25	0.87	2.87	0.83	0.56	1.64	1.19	1.36	2.28	0.84	1.85	0.99
BDE99MR	TCD	4.84	8.81	3.39	7.33	14.99	7.62	8.35	6.72	6.88	4.28	4.27	4.72	4.87	2.42
HAT707MR	TCD	5.99	7.17	4.86	6.25	13.76	6.57	6.66	6.44	6.47	5.42	5.25	5.93	5.41	3.48
TAE140MR	TCD	6.16	10.30	5.32	8.49	19.43	9.15	9.81	7.73	9.05	5.63	6.30	10.64	9.10	4.48
PlatonicHD6	TCD	29.13	9.02	11.78	9.12	15.25	6.07	7.92	12.91	13.87	13.89	25.53	12.18	20.40	15.80
PlatonicID6	TCD	19.35	13.21	12.04	14.37	14.45	11.42	12.03	10.14	9.32	10.80	16.65	5.68	10.03	18.37
PlatonicIG6	TCD	29.90	23.91	29.38	11.21	8.85	22.84	16.20	33.02	16.27	11.93	70.12	17.05	11.02	42.97
PlatonicTAE6	TCD	21.70	7.13	14.96	13.65	5.38	18.19	20.79	24.46	47.24	14.42	17.38	57.19	22.10	16.90
AE18	-	13.01	10.99	5.11	2.26	10.18	4.75	4.90	9.07	7.08	18.35	7.44	17.65	12.29	11.20

Table 7: RMSDs in kcal/mol for 8 barrier height datasets for the 14 Minnesota density functionals. BH stands for barrier heights. Table 2 contains specific information regarding the datasets, and the datatypes are explained in Section 3.

Dataset	Datatype	M05	M05-2X	M06	M06-2X	M06-HF	M08-HX	M08-SO	M11	MN12-SX	MN15	M06-L	M11-L	MN12-L	MN15-L
BHPERI26	BH	5.31	1.53	2.61	1.81	3.53	1.97	2.07	2.71	3.22	1.77	2.18	3.18	3.04	2.12
CRBH20	BH	7.84	2.77	8.74	1.58	9.56	1.31	1.80	1.25	3.97	1.09	13.73	9.70	6.55	7.18
DBH24	BH	3.35	1.63	2.87	1.08	3.44	1.30	1.20	1.42	1.75	1.82	5.24	3.46	2.50	3.22
CR20	BH	14.10	1.02	11.57	2.07	6.38	2.56	2.92	6.24	4.15	1.72	12.70	9.28	4.36	1.68
HTBH38	BH	2.39	1.65	2.31	1.29	2.44	1.25	1.47	1.73	1.44	1.38	4.66	2.14	1.80	1.81
NHTBH38	BH	3.17	1.85	2.74	1.67	3.42	1.57	1.65	1.49	1.97	2.55	4.86	3.83	3.08	3.46
PX13	BH	2.18	10.55	2.14	6.94	16.66	3.02	1.62	4.45	6.43	2.87	1.66	7.98	10.42	12.85
WCPT27	BH	2.10	3.92	2.09	3.42	6.46	1.79	1.39	2.25	2.38	2.24	2.24	3.18	3.17	4.38

Table 8: Equilibrium bond length (EBL) RMSDs in Å and equilibrium binding energy (EBE) RMSDs in kcal/mol for the 14 Minnesota density functionals. The first section contains the EBL RMSDs while the second section contains the EBE RMSDs. The All* category contains 81 data points and is a combination of BzDC215, NBC10, and S66x8. More information regarding the datasets and excluded potential energy curves can be found in Table 2 and Section 4.3, respectively.

Dataset	M05	M05-2X	M06	M06-2X	M06-HF	M08-HX	M08-SO	M11	MN12-SX	MN15	M06-L	M11-L	MN12-L	MN15-L
BzDC215	0.225	0.054	0.036	0.101	0.158	0.119	0.178	0.095	0.038	0.055	0.064	0.028	0.074	0.049
NBC10	0.836	0.115	0.158	0.091	0.150	0.114	0.131	0.076	0.073	0.081	0.099	0.061	0.179	0.134
RG10	0.214	0.137	0.539	0.247	0.365	0.353	0.315	0.673	1.182	0.095	0.311	1.379	1.304	0.095
S66x8	0.177	0.039	0.042	0.071	0.096	0.081	0.091	0.067	0.042	0.033	0.027	0.044	0.089	0.085
All* EBL	0.302	0.051	0.061	0.077	0.109	0.088	0.107	0.071	0.045	0.042	0.043	0.044	0.099	0.088
BzDC215	0.74	0.46	0.51	0.44	0.92	0.54	0.52	0.35	0.34	0.75	0.44	0.52	0.20	1.14
NBC10	1.88	0.99	0.84	0.46	0.59	0.48	0.41	0.82	0.87	0.39	0.75	0.86	0.79	1.62
RG10	0.10	0.07	0.13	0.11	0.10	0.14	0.13	0.17	0.18	0.03	0.14	0.34	0.19	0.02
S66x8	1.53	0.71	0.78	0.30	0.78	0.34	0.37	0.57	1.15	0.60	0.60	1.29	1.06	2.05
All* EBE	1.50	0.72	0.76	0.33	0.78	0.38	0.39	0.58	1.07	0.60	0.60	1.21	0.99	1.94

and MN12-L) or a double minimum (M11-L). All of the remaining functionals (except M08-HX, M08-SO, MN15, and MN15-L) overestimate the bond length of the krypton dimer by at least 0.1 Å, with M06, M06-2X, M06-HF, M11, and M06-L having bond lengths that are more than 0.4 Å too long. The EBE RMSDs for RG10 range from 0.02 to 0.34 kcal/mol, with the functionals underbinding the dimers in most cases. Not surprisingly, the three largest EBE RMSDs belong to MN12-SX, MN12-L, and M11-L, since these functionals barely bind the rare-gas dimers at all.

Moving on to the All* category, five functionals manage EBL RMSDs around 0.05 Å: MN15, M06-L, M11-L, MN12-SX, and M05-2X. The other two local functionals, MN15-L and MN12-L, perform more than 2 times worse than both M06-L and M11-L, with RMSDs of 0.088 and 0.099 Å, respectively. Three of the hybrid functionals perform very poorly, with M08-SO and M06-HF having RMSDs in excess of 0.1 Å, and M05 affording the worst overall result (0.302 Å). The rest of the hybrids (M06, M11, M06-2X, and M08-HX) manage RMSDs between 0.06 and 0.09 Å.

While MN15, M06-L, and M11-L are able to predict the most accurate bond lengths for these 81 PECs, their All* EBE RMSDs are quite poor, with M06-L and MN15 affording identical RMSDs of 0.60 kcal/mol and M11-L performing 2 times worse, with an RMSD of 1.21 kcal/mol. In comparison, the functional with the best EBE RMSD is M06-2X (0.33 kcal/mol), followed by M08-HX and M08-SO (0.38 and 0.39 kcal/mol, respectively). Unfortunately, these three functionals are unable to predict accurate bond lengths, with M06-2X having an EBL RMSD of 0.077 Å, followed by M08-HX (0.088 Å) and M08-SO (0.107 Å). Similarly, while MN12-SX performs reasonably well for the equilibrium bond lengths, its EBE RMSD is more than 1 kcal/mol. However, the worst equilibrium binding energies are attained by MN15-L, which has an All* EBE RMSD of almost 2 kcal/mol.

In fact, only 2 functionals (M06-L and MN15) manage to place in the top 50% with respect to both the All* EBL and All* EBE categories, with M06-L ranking second for bond lengths (0.043 Å) and fifth for binding energies (0.60 kcal/mol) and MN15 ranking first for bond lengths (0.042 Å) and sixth for binding energies (0.60 kcal/mol). Another good performer, M06-2X, is first for binding energies (0.33 kcal/mol) but only eighth for bond lengths (0.077 Å). Overall, none of the Minnesota functionals are able to accurately predict both equilibrium bond lengths and equilibrium binding energies for this set of 81 non-covalent interactions.

As an example of an interaction from the All* category, PECs of the benzene-silane dimer from BzDC215 are shown in Figure 2. Even with the (99,590) grid, the PECs for M06 and M06-L are visibly unconverged with respect to the grid. Five of the ten hybrid functionals predict bond lengths that are in error by at least 0.1 Å, with M05 having a bond length that is too long, and M06-2X, M06-HF, M08-HX, and M08-SO having bond lengths that are too short. None of the hybrid functionals are able to provide a satisfactory description of both the EBL and the EBE for this complex, since the five remaining hybrids underbind or overbind the dimer by at least 20%. As for the local functionals, the M06-L curve would be underbound (even if the grid issues were alleviated), and M11-L and MN12-L exhibit unphysical mid-range antibinding behavior. On the other hand, MN15-L drastically overbinds the dimer by almost 1 kcal/mol. Overall, none of the Minnesota functionals are able to satisfactorily describe the interaction between benzene and silane.

5 Reaching the Basis Set Limit

In order to assess the basis set convergence[125] of the Minnesota functionals for non-covalent interactions, 20 of the 21 equilibrium dimers from the A24 dataset were selected for analysis. The argon-ethene dimer was excluded since it was very difficult to converge this system for most of the functionals with the two quintuple-zeta basis sets. The results are sum-

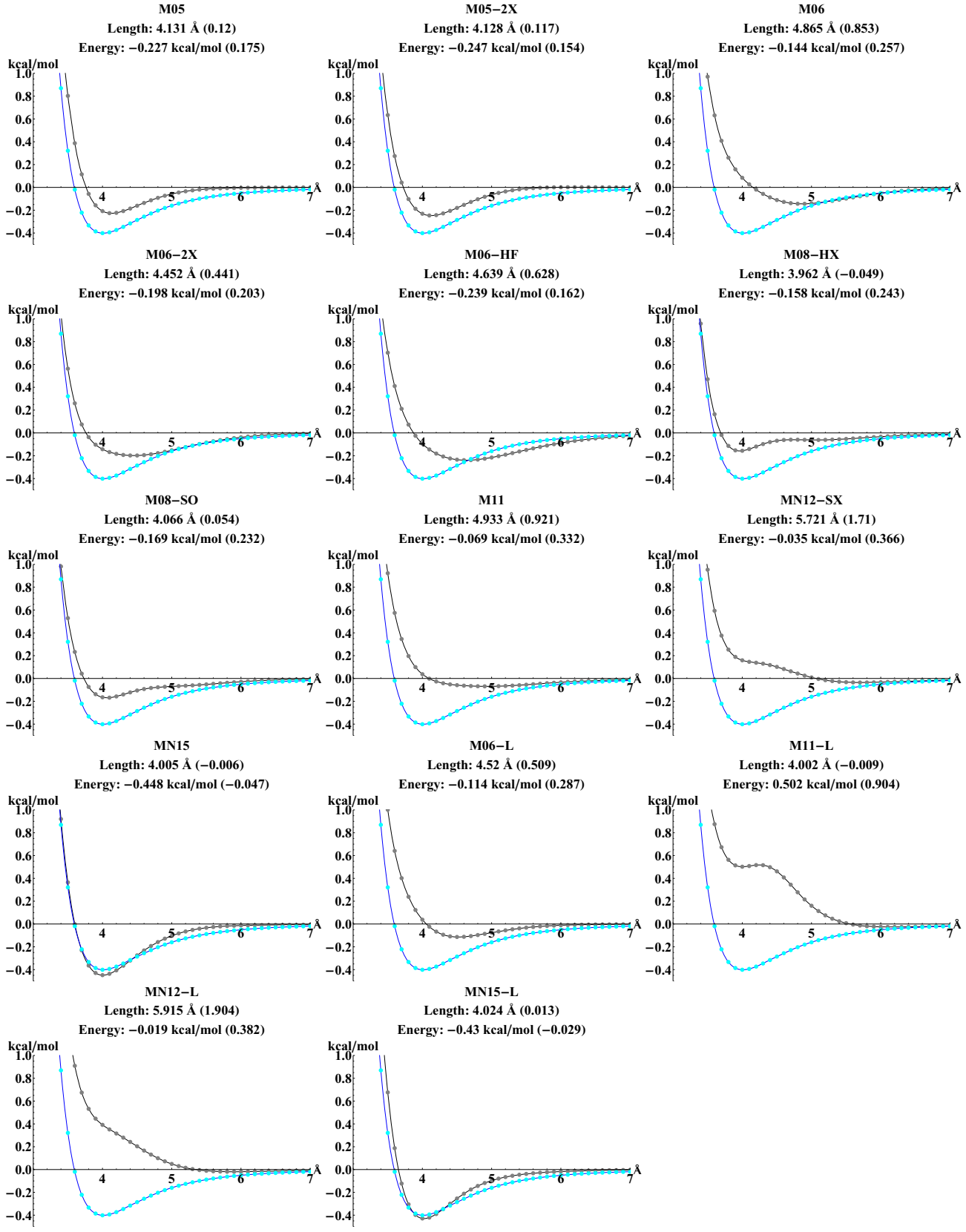

Figure 1: Potential energy curves for the krypton dimer from RG10 as computed by the 14 Minnesota density functionals. The gray curve represents the DFT method, while the blue curve represents the reference method. The line immediately following the functional name contains the equilibrium bond length in Å and the error (with respect to the reference) in parentheses. The following line contains the same information for the equilibrium binding energy (in kcal/mol).

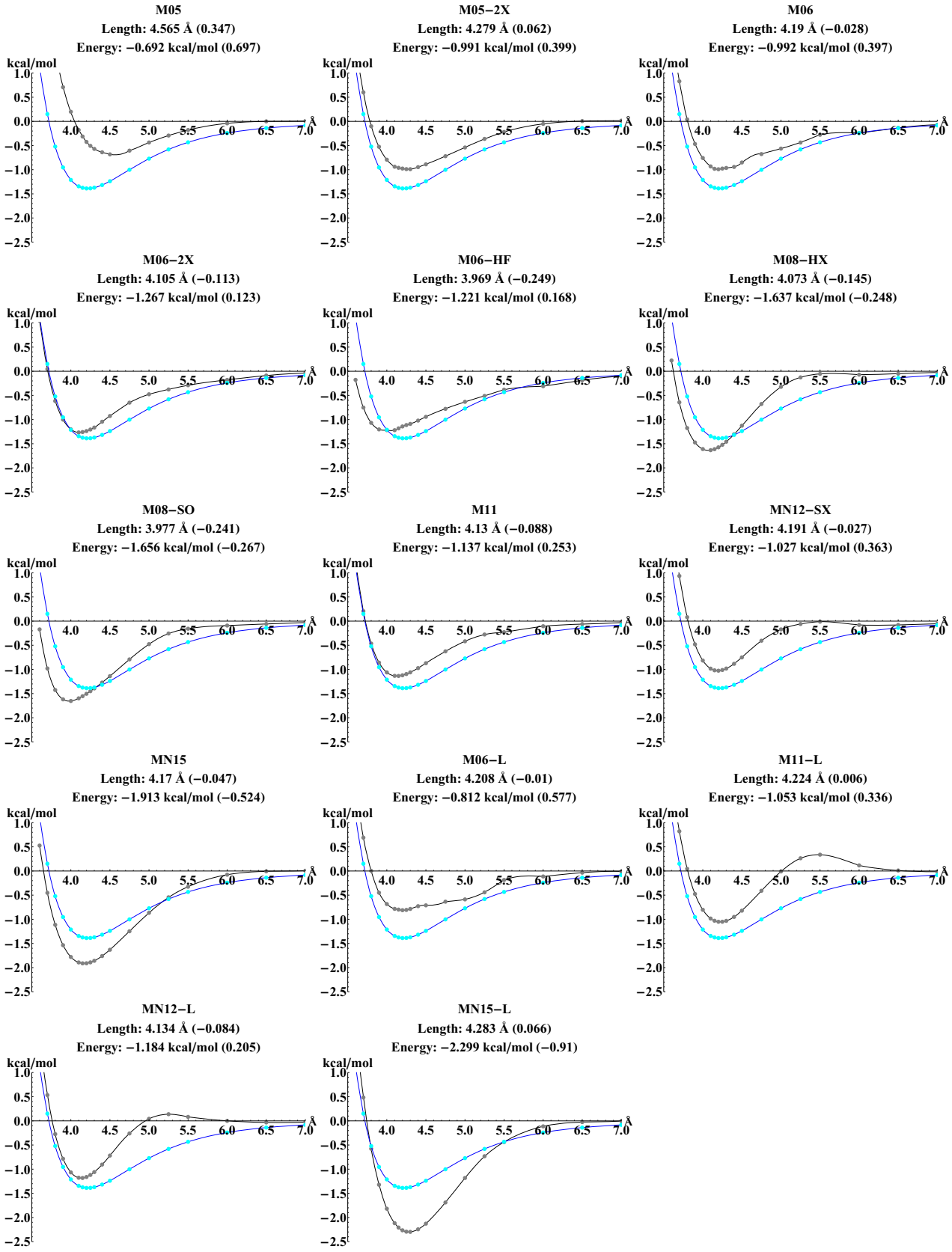

Figure 2: Potential energy curves for the benzene-silane dimer from BzDC215 as computed by the 14 Minnesota density functionals. The gray curve represents the DFT method, while the blue curve represents the reference method. The line immediately following the functional name contains the equilibrium bond length in Å and the error (with respect to the reference) in parentheses. The following line contains the same information for the equilibrium binding energy (in kcal/mol).

marized in Figure 3, which displays the mean absolute percent (MAP) basis set superposition error (BSSE) across the 20 dimers, relative to the A24 reference binding energies. The figure contains statistics for three Dunning basis sets, three Jensen basis sets, and two Karlsruhe basis sets, with the purple, orange, and green bars referring to the associated triple-zeta, quadruple-zeta, and quintuple-zeta basis sets, respectively. For comparison to the Minnesota functionals, results for two combinatorially-optimized density functionals that have kinetic energy density dependence (B97M-V,[123] a local meta-GGA with VV10 nonlocal correlation, and ωB97M-V,[126] a range-separated hybrid meta-GGA with VV10 nonlocal correlation) are presented as well.

Considering the popular Dunning series, it is interesting to note that none of the Minnesota functionals manage a MAP BSSE of less than 1% at the monstrous aug-cc-pV5Z basis set level. The only functionals that come close to this limit are M05-2X and M06-2X, with MAP BSSEs below 2%. On the other hand, the MAP BSSE of eight functionals (M06, M06-HF, MN12-SX, MN15, M06-L, M11-L, MN12-L, and MN15-L) is larger than 5% at the aug-cc-pV5Z basis set level, indicating that it is difficult to converge these functionals to the basis set limit. Of these eight functionals, M06-HF, M06-L, and MN12-L have MAP BSSEs larger than 10% at the aug-cc-pV5Z basis set level. In some cases (M06-HF, MN12-L, and MN15-L), the MAP BSSE does not monotonically decrease when going from aug-cc-pVTZ to aug-cc-pV5Z. Overall, only M05-2X and M06-2X are able to approach the basis set limit in a satisfactory manner with the Dunning basis sets. M05, M08-HX, M08-SO, and M11 have more difficulty reaching the basis set limit, with MAP BSSEs that are about 2 times larger than those of M05-2X and M06-2X in the quadruple- and quintuple-zeta basis sets. The remaining eight functionals display the most hardships with respect to reaching the basis set limit. In comparison, both B97M-V and ωB97M-V reach the basis set limit with greater ease, having MAP BSSEs of less than 1% at the aug-cc-pV5Z basis set level. Furthermore, both functionals have monotonically decreasing MAP BSSEs.

With the Jensen basis sets, the same conclusions mostly apply, with the main difference being that a monotonic decrease in the MAP BSSE is not witnessed for a majority of the Minnesota functionals (including M05-2X and M06-2X). Taking M06-2X as an example, the MAP BSSE drops from 4.26% in the aug-pc-2 basis set to 0.65% in the aug-pc-3 basis set, but then rises to 1.80% in the aug-pc-4 basis set. Considering the Karlsruhe basis sets, all of the functionals (except M06-HF) have a smaller MAP BSSE in def2-QZVPPD than def2-TZVPPD. In the def2-QZVPPD basis set, only M05, M05-2X, M06-2X, and MN15 have MAP BSSEs that are under 2%. Of the remaining 10 functionals, only M08-SO and MN15-L have a MAP BSSE under 5%, while the rest of the functionals lie between 5% and 15%. In def2-TZVPPD, the largest MAP BSSE belongs to M11 at 18.58%, while the smallest belongs to M06-2X, at 4.47%. In comparison, both B97M-V and ωB97M-V have monotonically decreasing MAP BSSEs in both the Jensen and Karlsruhe basis sets, and MAP BSSEs of at most 0.5% and 1% at the aug-pc-4 and def2-QZVPPD basis set levels, respectively. Based on these results, it appears that M05-2X and M06-2X are the two Minnesota functionals that have the most readily approachable basis set limit for non-covalent interactions using existing basis set sequences.

In order to assess the basis set convergence of the Minnesota functionals for thermochemistry, 27 of the 83 bond dissociation energies (BDE) from the BDE99nonMR dataset were selected for analysis. From the original set of 83, data points that included atomic energies were removed. Table 9 contains RMSDs for these 27 data points relative to the bond dissociation energies as calculated by each functional in the quintuple-zeta pc-4 basis set. In order to facilitate the discussion, the second column ranks the functionals from smallest to largest based on the geometric mean of the three quadruple-zeta basis set RMSDs.

Based on this measure, the most well-behaved functionals are ωB97M-V, M05-2X, M05, B97M-V, M06, M06-L, and MN15-L, while the most ill-behaved functionals are MN12-SX,

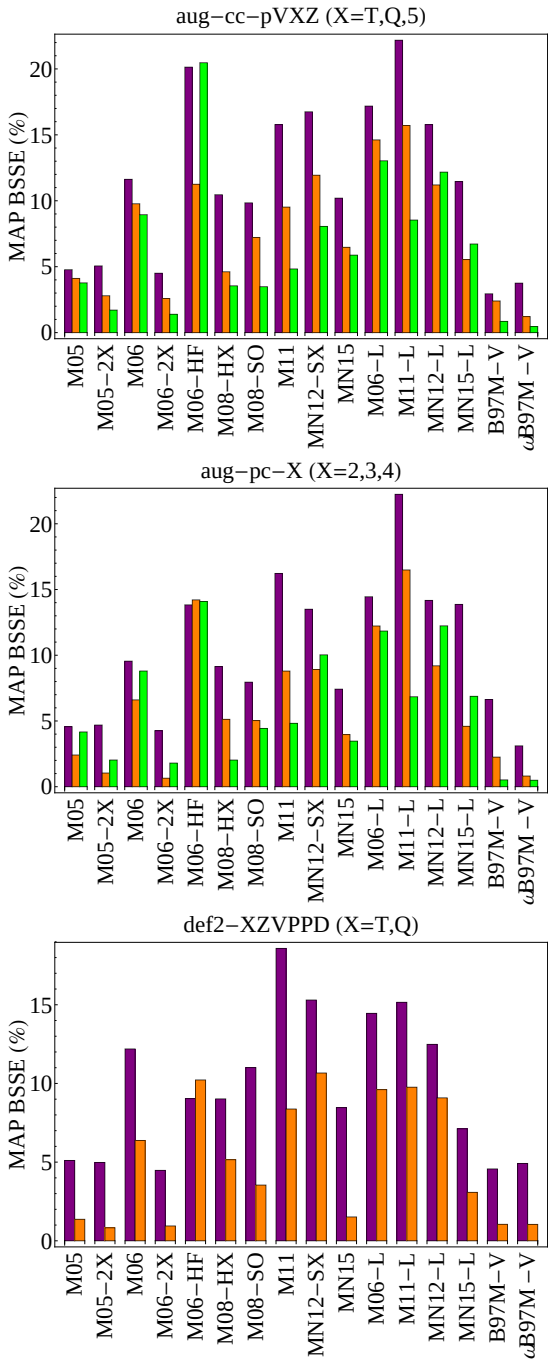

Figure 3: Mean absolute percent (MAP) basis set superposition errors (BSSE), relative to the A24 reference binding energies, for 20 of the 21 equilibrium complexes from the A24 dataset computed in 8 basis sets from 3 basis set families. The top figure corresponds to the Dunning basis sets, the middle figure corresponds to the Jensen basis sets, and the bottom figure corresponds to the Karlsruhe basis sets. The purple, orange, and green bars refer to the associated triple-zeta, quadruple-zeta, and quintuple-zeta basis sets, respectively.

M08-SO, M06-HF, and most strikingly, M11-L. The remaining functionals (M06-2X, M08-HX, MN15, M11, and MN12-L) appear to be sensitive to the choice of the quadruple-zeta basis set. For example, M06-2X has an RMSD of 0.70 kcal/mol in cc-pVQZ, but only 0.27 kcal/mol in def2-QZVPPD. Interestingly, the results suggest that the cc-pVQZ basis set is oftentimes less converged with respect to pc-4 than both def2-QZVPPD and pc-3. For example, the most well-behaved Minnesota functional, M05-2X, has an RMSD of 0.53 kcal/mol in cc-pVQZ, but only 0.14 kcal/mol in def2-QZVPP and 0.20 kcal/mol in pc-3. This trend is present for other well-behaved functionals such as ωB97M-V.

Based on these results, it appears that M11-L does not have a steadily approachable basis set limit for thermochemistry, and it is very likely that the pc-4 results do not represent the basis set limit for this functional. As an example of the poor convergence of M11-L towards the basis set limit, the BDE of C_2H_2 as predicted by M11-L is -228.38 kcal/mol in pc-2, -225.89 kcal/mol in pc-3, and -218.28 kcal/mol in pc-4. In stark contrast, the most well-behaved functional, ωB97M-V, has corresponding BDEs of -236.34, -235.56, and -235.40 kcal/mol. Similarly, M05-2X has corresponding BDEs of -238.57, -237.95, and -237.89 kcal/mol.

Across both sets of basis set limit tests, comparing MN12-L and MN15-L indicates that the inclusion of smoothness restraints in the design of MN15-L has helped to a noticeable extent. For example, the MAP BSSE of MN12-L in the aug-cc-pV5Z basis set is 12.17%, compared to 6.72% for MN15-L. However, even the MAP BSSE of MN15-L is unable to approach that of a functional with 46 fewer parameters (B97M-V with a MAP BSSE of 0.85%). Furthermore, for the 23 data points from BDE99nonMR, MN12-L ranks twelfth, while MN15-L ranks seventh. Thus, the smoothness restraints appear to help, to a certain extent, for bonded interactions as well.

Table 9: RMSDs in kcal/mol for 27 of the 83 bond dissociation energies from the BDE99nonMR dataset computed with nine basis sets. The reference values are taken to be the bond dissociation energies as calculated by each functional in the pc-4 basis set. The second column ranks the functionals from smallest (1) to largest (16) based on the geometric mean of the three quadruple-zeta basis set RMSDs.

Functional	Rank	cc-pVDZ	cc-pVTZ	cc-pVQZ	def2-SVP	def2-TZVPP	def2-QZVPP	pc-1	pc-2	pc-3
M05	3	3.12	0.57	0.34	4.60	0.37	0.19	3.59	0.66	0.24
M05-2X	2	1.98	0.47	0.53	3.80	0.43	0.14	2.96	0.39	0.20
M06	5	2.86	0.75	0.42	4.26	0.44	0.27	3.51	0.69	0.19
M06-2X	8	2.24	0.61	0.70	3.89	0.63	0.27	2.94	0.74	0.38
M06-HF	15	2.79	1.20	1.94	3.64	1.34	1.32	2.00	1.32	1.30
M08-HX	9	2.57	0.65	0.87	4.37	0.79	0.47	2.55	0.96	0.32
M08-SO	14	3.50	2.14	1.50	5.15	1.63	1.05	3.32	1.88	1.02
M11	11	2.83	0.78	0.97	4.55	1.42	0.75	2.98	1.08	0.62
MN12-SX	13	3.84	1.65	1.16	7.73	1.41	0.89	5.38	2.10	0.86
MN15	10	3.53	1.28	0.97	5.85	1.19	0.31	2.77	0.87	0.62
M06-L	6	2.93	0.69	0.42	4.59	0.43	0.33	3.93	0.74	0.20
M11-L	16	5.10	3.19	3.67	11.65	4.47	1.97	6.58	4.75	3.29
MN12-L	12	3.91	1.51	0.69	8.43	1.36	0.91	4.90	1.49	0.84
MN15-L	7	2.86	1.33	0.51	4.59	0.48	0.29	4.20	1.10	0.20
B97M-V	4	2.25	0.68	0.38	4.25	0.19	0.21	3.36	0.61	0.24
ωB97M-V	1	2.39	0.72	0.43	4.59	0.36	0.10	2.44	0.42	0.09

6 Reaching the Integration Grid Limit

While meta-GGA functionals have the potential of being significantly more accurate than their GGA counterparts for a variety of applications, an unfortunate disadvantage of meta-GGA functionals is that the evaluation of the kinetic energy density is highly sensitive to the choice of integration grid, particularly for semi-empirical functionals such as the Minnesota functionals[119–121] or exchange-correlation functionals based on the B95 correlation functional.[120] While this side-effect has been explored thoroughly by several authors in the past, only a subset of the Minnesota functionals have been analyzed. Nevertheless, the developers of the Minnesota functionals recommend using at least an ultrafine (99,590) grid in order to avoid integration errors.

In order to consistently assess the grid sensitivity of all of the Minnesota density functionals for non-covalent interactions, the benzene-neon dimer potential energy curve from the BzDC215 dataset was selected as a model non-covalent interaction, and the 24 associated data points were calculated with nine different grids, formed from the combination of three radial {99, 250, 500} and three angular {590, 770, 974} choices. Figure 4 contains three bar charts that display the RMSD of the 24 data points in the given grid with respect to the finest grid utilized, the (500,974) grid. This is done separately for different numbers of radial shells, namely 99, 250, and 500, while within each subfigure, the number of angular grid points per shell is modified (purple is 590, orange is 770, and green is 974).

For comparison to the Minnesota functionals, results for two combinatorially-optimized, meta-GGA density functionals (B97M-V and ωB97M-V) are presented as well. It is visually evident from Figure 4 that the grid sensitivity of the Minnesota functionals varies greatly from one functional to another. While none (besides M11-L) are as insensitive to the grid as B97M-V and ωB97M-V, a majority of the Minnesota

functionals appear to be acceptably converged in the (99,590) grid, with the exception of M06, M06-HF, M11, MN12-SX, M06-L, and MN12-L.

Considering the data for 99 radial shells, it appears that changing the number of angular grid points per shell is not very helpful for any of the functionals considered. M06 stands out as being the most sensitive, with an RMSD of over 100 cal/mol when 99 radial shells are employed. The most sensitive local functional is M06-L, with an RMSD of around 60 cal/mol, which is about 25 times larger than that of M11-L. From the hybrid functionals, M06-HF, M11, and MN12-SX are problematic as well, while M05, M05-2X, M06-2X, M08-HX, M08-SO, and MN15 have the smallest deviations from the (500,974) values. While MN12-L and MN15-L are less sensitive to the grid than M06-L, their grid error RMSDs are still on par with some of the problematic hybrids.

When the number of radial shells is upgraded from 99 to 250, M06 and M06-L are still the most problematic hybrid and local functionals, respectively. However, varying the number of angular grid points per shell does seem to have an ameliorating effect for some functionals, namely M08-SO, M11-L, and MN12-L. Nevertheless, most of the functionals are converged to within 1 cal/mol by (250,590), which is a quantity that is not visibly discernible on a PEC plot. Finally, with 500 radial shells, all of the functionals are converged to within 1 cal/mol.

Figure 5 plots the benzene-neon potential energy curves for all 16 functionals in the (99,590) grid (red, dashed) and the (500,974) grid (blue), along with the reference PEC from BzDC215 (black). These plots make it clear that of the hybrid functionals, M06, M06-HF, M11, and MN12-SX are unacceptably oscillatory in the (99,590) grid, while from the local functionals, M06-L and MN12-L are unacceptably oscillatory in the (99,590) grid. Considering the blue curves, it is evident that MN12-SX, M11-L, and MN12-L have the same strange behavior that was witnessed for the krypton dimer, indicating that these functionals are incapable of even qualitatively describing weakly-interacting

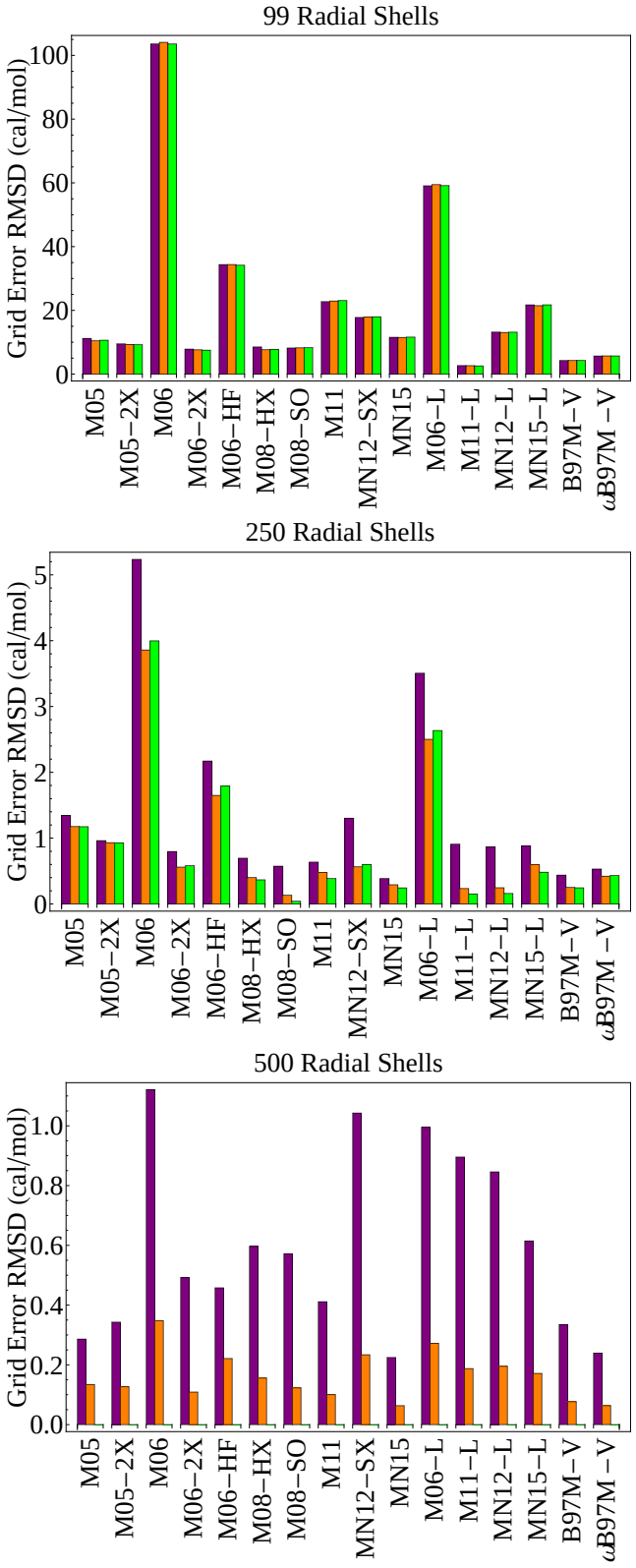

Figure 4: RMSDs for the 24 points on the benzene-neon dimer potential energy curve with respect to the (500,974) grid. The subfigures correspond to a fixed number of radial shells, and within each subfigure, the number of angular grid points is varied (purple is 590, orange is 770, and green is 974).

molecules that are primarily bound by dispersion. Besides these three functionals, the rest of the Minnesota functionals (except M06) severely overestimate the equilibrium binding energy of the benzene-neon dimer, with the most drastic overbinding achieved by MN15-L.

The sensitivity of the Minnesota density functionals to the integration grid for thermochemistry is explored with the 19 atomization energies from the AlkAtom19 dataset, and the results are summarized in Table 10. The RMSDs are taken with respect to the (500,974) integration grid, and it is clear that all of the considered functionals are certainly converged in the (99,590) grid. In fact, even the (75,302) appears to be sufficient for most of the functionals, perhaps with the exception of M06-HF and M06-L. In accordance with expectation, the SG-1 grid introduces large errors in these atomization energies and should be avoided in most cases. The unpruned version of SG-1, (50,194), does not improve much upon SG-1, and it is evident that a grid of at least (75,302) quality should be the minimum used for these meta-GGA functionals.

Within both sets of integration grid limit tests, comparing MN12-L and MN15-L indicates that the inclusion of smoothness restraints in the design of MN15-L has had a minor effect. For example, the grid error RMSD of MN15-L for the benzene-neon dimer is larger than that of MN12-L. However, this is due to the fact that MN15-L severely overbinds this system, and when the potential energy curves in Figure 5 are considered, it is evident that MN15-L is slightly less oscillatory than MN12-L. For the atomization energies from AlkAtom19, however, there is no difference between MN12-L and MN15-L for the two grids that are useful for meta-GGAs: (75,302) and (99,590).

Table 10: RMSDs in kcal/mol for the 19 atomization energies from the AlkAtom19 dataset computed with 4 integration grids. The reference values are taken to be the atomization energies as calculated by each functional with the (500,974) integration grid.

Functional	SG-1	(50,194)	(75,302)	(99,590)
M05	1.45	0.38	0.03	0.00
M05-2X	1.64	1.53	0.12	0.01
M06	0.73	0.33	0.09	0.00
M06-2X	2.08	1.71	0.09	0.01
M06-HF	5.00	2.84	0.38	0.02
M08-HX	2.17	2.06	0.14	0.01
M08-SO	1.20	0.83	0.06	0.01
M11	1.18	1.27	0.07	0.00
MN12-SX	0.35	0.31	0.04	0.00
MN15	0.20	0.08	0.02	0.00
M06-L	0.66	0.80	0.28	0.02
M11-L	2.64	3.77	0.11	0.02
MN12-L	0.40	0.27	0.04	0.00
MN15-L	0.21	0.13	0.04	0.00
B97M-V	0.34	0.23	0.02	0.00
ωB97M-V	0.08	0.07	0.01	0.00

7 Discussion

Although this study is primarily concerned with benchmarking the Minnesota functionals, it is difficult to provide perspective to these results if the Minnesota functionals are solely being compared among themselves. For ex-

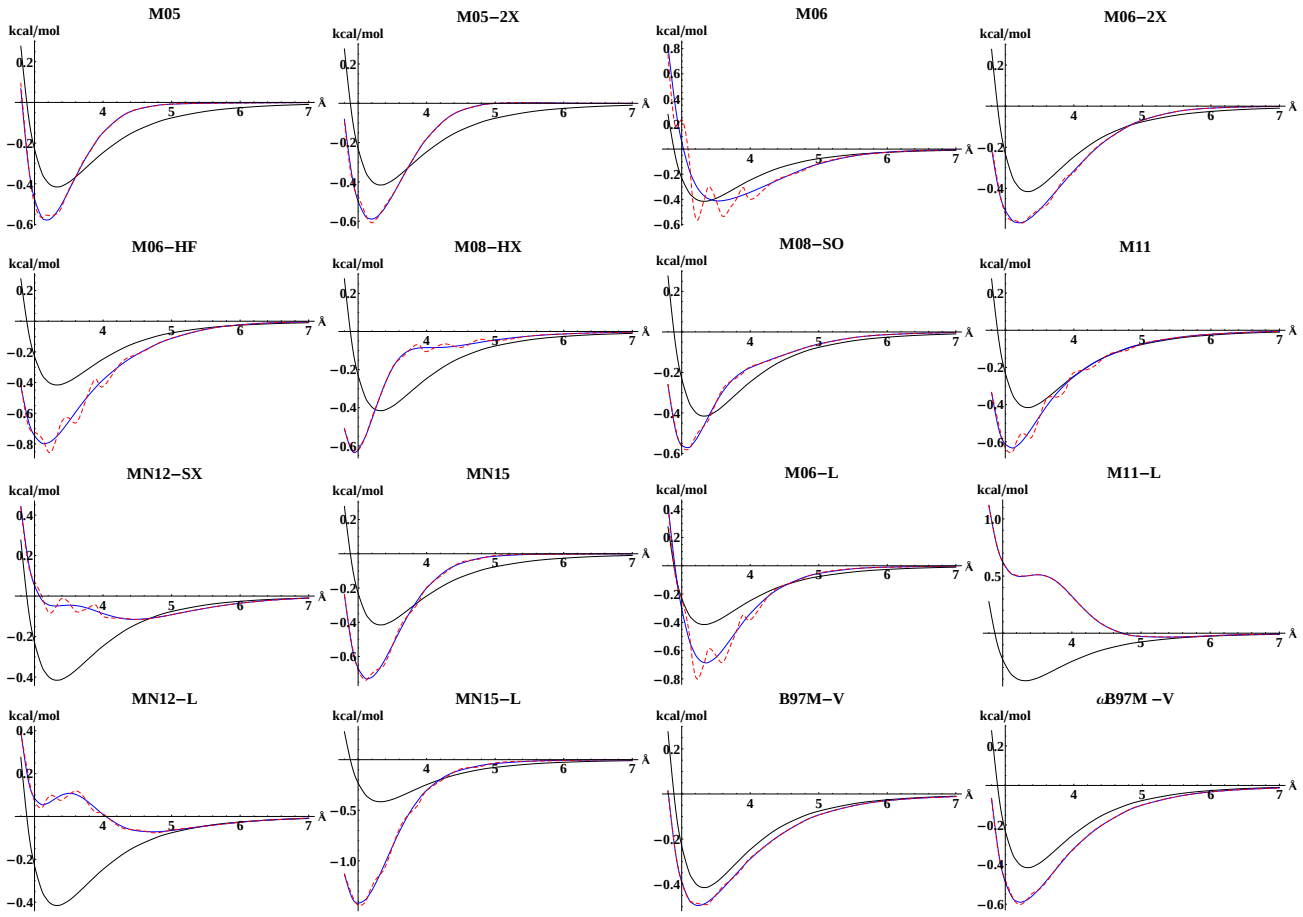

Figure 5: Potential energy curves for the benzene-neon dimer from BzDC215 as computed by the 14 Minnesota density functionals, B97M-V, and ωB97M-V. The red, dashed curve represents the DFT method evaluated in the (99,590) grid, the blue curve represents the DFT method evaluated in the (500,974) grid, and the black curve represents the reference potential energy curve.

ample, while M06-2X has the smallest RMSD of 0.43 kcal/mol for the NCED datatype, it is not clear if this is an overall positive result, or if this is a positive result because only the Minnesota functionals are being considered. *In order to properly address this issue, results from another project which benchmarked an additional 127 density functionals on the entire database were employed to provide meaningful comparisons within each category.* The full list of benchmarked functionals can be found in the Supporting Information. Since this discussion as well as the following conclusions will heavily utilize the datatypes, the eight acronyms will be repeated here in order to facilitate the analysis: NCED (non-covalent dimers (easy)), NCEC (non-covalent clusters (easy)), NCD (non-covalent dimers (difficult)), IE (isomerization energies (easy)), ID (isomerization energies (difficult)), TCE (thermochemistry (easy)), TCD (thermochemistry (difficult)), and BH (barrier heights). As a further reminder, "easy" refers the systems that are not heavily influenced by strong correlation or self-interaction error.

It is important to highlight the fact that the Minnesota functionals are being considered without any dispersion corrections. One reason for this is that four of the functionals (M08-HX, M08-SO, MN15, and MN15-L) do not have existing DFT-D3 parameters. Another reason is that none of the 12 papers mention or utilize any of the existing parameterizations. Additionally, since the Minnesota functionals have been trained using a database that contains datasets that include non-covalent interactions, some of them already overbind these types of interactions, and the addition of a dispersion tail tends to worsen this overbinding. For example, for M06-2X and M06-2X-D3(0), the NCED RMSDs are 0.43 and 0.35 kcal/mol, respectively, while the NCEC RMSDs are 2.52 and 3.19 kcal/mol, respectively. Thus, while the addition of the dispersion tail helps slightly for dimers (most significantly with the dispersion-bound cases), it worsens the overbinding of species such as hydrogen-bonded water clusters.

Tables 11 and 12 summarize the performance of the hybrid and local Minnesota functionals, respectively, for the eight datatypes (as well as the All* EBL and All* EBE categories), and additionally provide results for the top contender in each category from among all 141 benchmarked density functionals. It is important to mention that this comparison does not include the three recent functionals developed by the present authors (ωB97X-V,[122] B97M-V, and ωB97M-V), since these functionals were partially trained using the employed database. However, results for comparison can be found in Reference 126 for interested readers.

Starting with the NCED datatype, the best hybrid Minnesota functional is M06-2X with an RMSD of 0.43 kcal/mol, while the best overall hybrid functional is B3LYP-D3(CSO)[4–6,127–129] with an RMSD of 0.30 kcal/mol. Additionally, the best local Minnesota functional is M06-L with an RMSD of 0.55 kcal/mol, while the best overall local functional is BLYP-D3(BJ)[4,5,127,128] with an RMSD of 0.34 kcal/mol. Thus, the best hybrid Minnesota functional performs more than 40% worse than B3LYP utilizing a modified DFT-D3 dispersion correction[129] that only includes C_6 terms, while the best local Minnesota functional performs more than 60% worse than BLYP utilizing the DFT-D3 dispersion correction with BJ-damping.[128] These results indicate that none of the Minnesota functionals are well-suited for predicting the binding energies of traditional non-bonded dimers. This outcome is not entirely surprising, since non-covalent interactions have had a small presence in the databases used to train the Minnesota functionals.

Moving on to the NCEC datatype, the best hybrid Minnesota functional is M08-HX with an RMSD of 1.73 kcal/mol, while the best overall hybrid functional is ωB97X-D[130] with an RMSD of 1.01 kcal/mol. Additionally, the best local Minnesota functional is M06-L with an RMSD of 2.20 kcal/mol, while the best overall local functional is MGGA_MS1-D3(0)[127,131] with an RMSD of 0.81 kcal/mol. Thus, the best Minnesota functional (M08-HX) is still more than 2 times worse than the best overall functional (MGGA_MS1-D3(0)). The poor performance of the Minnesota density functionals for

these types of interactions is certainly not surprising, since none of the 14 functionals have been trained on non-covalent clusters.

The NCD datatype, which is strongly associated with self-interaction error, is a strong suit for Minnesota functionals with large fractions of exact exchange. Consequently, the best overall density functional for NCD is M08-SO (0.91 kcal/mol), which contains 56.79% exact exchange and is, in fact, the Minnesota functional with the largest fraction of exact exchange (besides M06-HF). Not surprisingly, other Minnesota functionals that can approach the performance of M08-SO for these interactions are fellow functionals with large fractions of exact exchange, namely MN15 (44%), M06-2X (54%) and M08-HX (52.23%). This result means that these Minnesota functionals are the best available functionals for applications of this type, if double hybrids or self-interaction-free wave function methods are not affordable.

Considering the IE datatype, the best hybrid Minnesota functional, M05-2X, ties with the best overall hybrid functional (ωM06-D3[132]), with an RMSD of 0.41 kcal/mol. On the other hand, the best local Minnesota functional, M11-L, with an RMSD of 0.69 kcal/mol, performs 50% worse than the best overall local functional, MGGA_MS2-D3(0)[127,131] (0.46 kcal/mol). Thus, the performance of M05-2X is noteworthy, as the next best Minnesota functional (M06-2X) is already 20% worse.

Similar to the NCD datatype, the ID datatype contains isomerization energies that are highly susceptible to self-interaction error. The best hybrid Minnesota density functional is M08-SO with an RMSD of 3.95 kcal/mol, which is 30% worse than the best overall hybrid functional, ωB97X-D3[132] (3.02 kcal/mol). Similarly, the best local Minnesota functional, M11-L, with an RMSD of 5.99 kcal/mol, performs about 30% worse than the best overall local functional, SCAN[133] (4.74 kcal/mol).

Moving on to bonded interactions with the TCE datatype, the best hybrid Minnesota functional is M06-2X, with an RMSD of 3.29 kcal/mol, while the best overall hybrid functional is PW6B95-D3(0) with an RMSD of 3.16 kcal/mol. Thus, M06-2X almost matches the performance of the best benchmarked density functional. Newer functionals such as M08-HX, M11, and MN15 are slightly (10-15%) poorer. As for the local functionals, MN15-L, with an RMSD of 4.62 kcal/mol, is both the best local Minnesota functional as well as the best overall local functional. In comparison, M06-L is roughly 20% poorer.

Unlike the TCE datatype, the TCD datatype contains bonded interactions that are either multi-reference in nature or prone to self-interaction error. The best hybrid Minnesota functional is MN15 with an RMSD of 6.44 kcal/mol, while the best overall hybrid functional is revPBE0-D3(BJ)[7,8,127,128,134] with a 20% smaller RMSD of 5.06 kcal/mol. Moving on to the local functionals, MN12-L, with an RMSD of 7.47 kcal/mol, is the best local Minnesota functional, while SCAN is the best overall local functional, with an RMSD of 6.41 kcal/mol.

For the BH datatype, the best hybrid Minnesota density functional, M08-SO (1.78 kcal/mol), is also the best overall hybrid density functional. Clearly, M08-SO, as well as M08-HX and MN15, are state-of-the-art functionals for the types of barrier heights included in this benchmark. Of the local functionals, MN12-L (4.29 kcal/mol) is both the best local Minnesota functional as well as the best overall local functional. However, none of the local functionals can approach the performance of the best hybrids, since this property is significantly improved by the inclusion of exact exchange.

Finally, considering the equilibrium properties discussed in Section 4.3, the best hybrid Minnesota functional for non-rare-gas dimer equilibrium bond lengths is MN15 with an RMSD of 0.042 Å, while the best overall hybrid functional is B3LYP-D3(BJ)[4–6,127,135] with an RMSD of 0.022 Å. Thus, the RMSD of MN15 is almost 2 times bigger than that of a standard hybrid GGA utilizing a dispersion correction. However, the best hybrid Minnesota functional for non-rare-gas dimer equilibrium binding energies, M06-2X, has an RMSD (0.33 kcal/mol) that is on par with that of the best overall hybrid functional, PW6B95-D3(CSO) (0.26

kcal/mol). Considering the local functionals, M06-L, with an RMSD of 0.043 Å, is the best-performing Minnesota functional, but performs more than 1.5 times worse than VV10 (0.028 Å). M06-L is also the best-performing local Minnesota functional for the non-rare-gas dimer equilibrium binding energies, but performs almost 2.5 times worse than BLYP-D3(BJ) for the 81 associated data points. These results further indicate that none of the Minnesota functionals are competitive with the best available functionals for describing interactions between traditional non-bonded dimers.

8 Conclusions

The ultimate goal of this study is to identify the Minnesota functionals that are state-of-the-art for the types of systems contained in the present database. In order to accomplish this task, a large database of 4986 data points was utilized, over 4 times larger than Grimme's GMTKN30 database[102] (841 data points) and Truhlar's CE345 database[24] (345 data points), combined. It is also more than 10 times larger than the Database 2015A (422 data points) used for the development of MN15-L. Thus, the results of this benchmark and the ensuing conclusions should be transferable to other related applications of the Minnesota functionals. In addition to benchmarking the performance of these functionals on energetics, 90 interpolated potential energy curves were analyzed to assess the accuracy of these functionals for predicting equilibrium bond lengths and equilibrium binding energies of non-covalent dimers. Furthermore, the functionals were assessed with respect to their sensitivity to the choice of basis set, as well as integration grid.

Tables 13 and 14 are useful in achieving the aforementioned goal, as they list the percentage of datasets (categorized by datatype) for which the RMSD of a given functional is within 25% of the best possible across all of the benchmarked functionals in its class. For the hybrid functionals, this includes a total of 73 functionals, while for the local functionals, this includes a total of 68 functionals. With the help of these two tables, as well as Tables 11 and 12, some overall recommendations will be made (although these generalizations are not meant as substitutes for a detailed study of the data provided, and are subject to caveats that will be mentioned later).

Considering the ten hybrid Minnesota functionals, it is clear that none of them are state-of-the art for the NCED and NCEC datasets, while only M05-2X appears to be at a desirable level of accuracy for the IE datasets. Most of the hybrids with a high fraction ($> 40\%$) of exact exchange are state-of-the-art for the NCD datasets, with the notable exception of M05-2X, M06-HF, and M11. As expected, M06-2X is very accurate for the TCE datasets, while M08-HX, M11, and MN15 have noteworthy performances as well. While none of the hybrids are state-of-the-art for the TCD datasets, it is important to mention that M06 and MN15 are good options for the types of multi-reference interactions contained in the W4-11 database. Finally, the hybrid Minnesota density functionals have historically been very useful for barrier heights, and both 2008 Minnesota functionals, as well as MN15 and M06-2X are very good for the BH datatype. While the hybrid Minnesota functionals perform poorly for the NCED and NCEC datasets relative to the best benchmarked hybrid functionals, if a hybrid Minnesota functional must be used for such interactions, then MN15 (or M06-2X) is perhaps the safest choice.

Considering the four local Minnesota functionals, it is clear that none of them are state-of-the-art for the easy non-covalent interactions (NCED and NCEC) and isomerization energy (IE) datasets. However, MN12-L and MN15-L are quite accurate for the NCD datasets, which primarily contain open-shell non-covalent dimers that are heavily characterized by electron delocalization. Additionally, M11-L, MN12-L, and MN15-L are satisfactory for the ID datasets, which primarily contain isomerization energies that are prone to self-interaction error. For the TCE datasets, MN15-L is certainly state-of-the-art, and the performance of MN12-L is also noteworthy. Additionally, MN15-L performs very well for the three multi-reference datasets in the TCD datatype,

Table 11: RMSDs for the 8 datatypes (as well as the All* EBL and All* EBE categories) for the 10 hybrid Minnesota density functionals and the top contender in each category from among all 73 benchmarked hybrid density functionals.

Datatype	M05	M05-2X	M06	M06-2X	M06-HF	M08-HX	M08-SO	M11	MN12-SX	MN15	Best	Functional
NCED	1.53	0.67	0.71	0.43	0.82	0.58	0.56	0.65	0.99	0.47	0.30	B3LYP-D3(CSO)
NCEC	3.85	2.44	2.88	2.52	4.97	1.73	2.14	2.82	8.61	1.83	1.01	ωB97X-D
NCD	1.55	1.55	1.54	0.99	1.95	1.03	0.91	1.23	1.57	0.96	0.91	M08-SO
IE	1.13	0.41	0.77	0.50	0.61	0.59	0.71	0.74	0.61	0.71	0.41	ωM06-D3
ID	8.67	4.66	8.17	5.56	5.89	4.62	3.95	5.65	6.37	4.06	3.02	ωB97X-D3
TCE	5.48	3.98	4.11	3.29	5.82	3.60	4.03	3.67	5.46	3.76	3.16	PW6B95-D3(0)
TCD	9.59	8.49	7.27	7.23	14.08	8.14	8.12	9.19	10.26	6.44	5.06	revPBE0-D3(BJ)
BH	5.83	3.41	5.05	2.57	6.48	1.80	1.78	2.82	3.05	1.98	1.78	M08-SO
All* EBL	0.302	0.051	0.061	0.077	0.109	0.088	0.107	0.071	0.045	0.042	0.022	B3LYP-D3(BJ)
All* EBE	1.50	0.72	0.76	0.33	0.78	0.38	0.39	0.58	1.07	0.60	0.26	PW6B95-D3(CSO)

Table 12: RMSDs for the 8 datatypes (as well as the All* EBL and All* EBE categories) for the 4 local Minnesota density functionals and the top contender in each category from among all 68 benchmarked local density functionals.

Datatype	M06-L	M11-L	MN12-L	MN15-L	Best	Functional
NCED	0.55	1.18	1.08	1.38	0.34	BLYP-D3(BJ)
NCEC	2.20	9.47	11.65	12.83	0.81	MGGA_MS1-D3(0)
NCD	1.87	1.65	1.29	1.45	1.29	MN12-L
IE	0.71	0.69	1.06	1.55	0.46	MGGA_MS2-D3(0)
ID	10.16	5.99	7.93	6.94	4.74	SCAN
TCE	5.44	7.22	4.95	4.62	4.62	MN15-L
TCD	12.97	11.09	7.47	8.62	6.41	SCAN
BH	6.85	5.39	4.29	4.78	4.29	MN12-L
All* EBL	0.043	0.044	0.099	0.088	0.028	VV10
All* EBE	0.60	1.21	0.99	1.94	0.25	BLYP-D3(BJ)

making it the best (and only) choice for such interactions. Finally, as far as local functionals are considered, MN15-L is state-of-the-art for BH, as is MN12-L. While the four local Minnesota functionals perform poorly for the NCED, NCEC, and IE datasets relative to the best benchmarked local functionals, if a local Minnesota functional must be used for such interactions, then M06-L is the obvious choice, since the three newest local functionals are quite unsuitable for these datatypes (with the exception of M11-L for IE).

While the database used to assess the Minnesota density functionals in this study contains nearly 5000 data points, it is important to point out a few limitations of this work and its conclusions. First and most important, this assessment is limited to molecules composed of main-

Table 13: Percentage of datasets (categorized by datatype) for which the RMSD of a given functional is within 25% of the best possible across the 73 benchmarked hybrid density functionals. As an example, from among the 15 TCE datasets, M06 is within 25% of the best possible RMSD for only 7% (or 1) of the 15 datasets. The number of datasets in each datatype is 18 (NCED), 12 (NCEC), 5 (NCD), 12 (IE), 5 (ID), 15 (TCE), 7 (TCD), and 8 (BH), respectively. The datatypes are explained in Section 3.

Functional	NCED	NCEC	NCD	IE	ID	TCE	TCD	BH
M05	0	0	0	0	0	0	0	0
M05-2X	0	17	0	33	0	7	0	25
M06	6	0	0	0	0	7	14	0
M06-2X	0	0	20	0	20	40	0	38
M06-HF	0	0	20	0	0	0	0	0
M08-HX	0	8	20	0	20	20	0	38
M08-SO	0	0	20	0	40	33	0	50
M11	0	0	0	0	0	20	0	13
MN12-SX	0	0	20	0	0	20	0	13
MN15	6	0	40	0	0	33	0	13

Table 14: Percentage of datasets (categorized by datatype) for which the RMSD of a given functional is within 25% of the best possible across the 68 benchmarked local density functionals. As an example, from among the 15 TCE datasets, M06-L is within 25% of the best possible RMSD for only 13% (or 2) of the 15 datasets. The number of datasets in each datatype is 18 (NCED), 12 (NCEC), 5 (NCD), 12 (IE), 5 (ID), 15 (TCE), 7 (TCD), and 8 (BH), respectively. The datatypes are explained in Section 3.

Functional	NCED	NCEC	NCD	IE	ID	TCE	TCD	BH
M06-L	0	17	20	8	0	13	0	38
M11-L	0	0	20	8	40	13	0	25
MN12-L	0	0	60	0	40	27	0	38
MN15-L	6	0	40	0	40	60	43	50

group elements, and recent Minnesota functionals are trained using a diverse database that includes systems outside the scope of the present benchmark, such as the multi-reference transition metal bond energies of Cr_2, V_2, and Fe_2. It will be useful to systematically assess the performance of the Minnesota functionals on transition metals, solid state materials, and other multi-reference interactions in the future, as accurate reference values become available. For such systems, training set results indicate that the MN15-L functional is a promising choice. Second, this assessment was limited to ground state properties, and excluded excitation energies. For instance, the M06-HF functional was designed to be accurate for charge-transfer excitation energies accessed through the TDDFT approach, and this strength does not appear in the present database. Nevertheless, since several recent benchmarks utilize M06-HF for datasets that are heavily characterized by self-interaction error,[92,94] benchmarking M06-HF along with the rest of the Minnesota functionals is certainly useful for the electronic structure community. Third, the results and conclusions presented here are meant to be used as a general guide, and are not intended to replace specific recommendations from specific benchmarking studies.

9 Associated Content

A full list of all 141 benchmarked functionals is provided. This information is available free of charge via the Internet at http://pubs.acs.org.

10 Acknowledgements

This work was supported by the Director, Office of Energy Research, Office of Basic Energy Sciences, Chemical Sciences Division of the U.S. Department of Energy under Contract DE-AC0376SF00098, and by a grant from the SciDac Program.

References

(1) Kohn, W.; Sham, L. J. Self-Consistent Equations Including Exchange and Correlation Effects. *Phys. Rev.* **1965**, *140*, A1133–A1138.

(2) Ruzsinszky, A.; Perdew, J. P. Twelve outstanding problems in ground-state density functional theory: A bouquet of puzzles. *Comp. Theor. Chem.* **2011**, *963*, 2 – 6.

(3) Cohen, A. J.; Mori-Sánchez, P.; Yang, W. Challenges for Density Functional Theory. *Chem. Rev.* **2012**, *112*, 289–320.

(4) Becke, A. D. Density-functional exchange-energy approximation with correct asymptotic behavior. *Phys. Rev. A* **1988**, *38*, 3098–3100.

(5) Lee, C.; Yang, W.; Parr, R. G. Development of the Colle-Salvetti correlation-energy formula into a functional of the electron density. *Phys. Rev. B* **1988**, *37*, 785–789.

(6) Becke, A. D. Density-functional thermochemistry. III. The role of exact exchange. *J. Chem. Phys.* **1993**, *98*, 5648–5652.

(7) Perdew, J. P.; Burke, K.; Ernzerhof, M. Generalized Gradient Approximation Made Simple. *Phys. Rev. Lett.* **1996**, *77*, 3865–3868.

(8) Adamo, C.; Barone, V. Toward reliable density functional methods without adjustable parameters: The PBE0 model. *J. Chem. Phys.* **1999**, *110*, 6158–6170.

(9) Zhao, Y.; Truhlar, D. G. A new local density functional for main-group thermochemistry, transition metal bonding, thermochemical kinetics, and noncovalent interactions. *J. Chem. Phys.* **2006**, *125*, 194101.

(10) Peverati, R.; Truhlar, D. G. M11-L: A Local Density Functional That Provides Improved Accuracy for Electronic Structure Calculations in Chemistry and Physics. *J. Phys. Chem. Lett.* **2012**, *3*, 117–124.

(11) Peverati, R.; Truhlar, D. G. An improved and broadly accurate local approximation to the exchange-correlation density functional: The MN12-L functional for electronic structure calculations in chemistry and physics. *Phys. Chem. Chem. Phys.* **2012**, *14*, 13171–13174.

(12) Yu, H. S.; He, X.; Truhlar, D. G. MN15-L: A New Local Exchange-Correlation Functional for Kohn–Sham Density Functional Theory with Broad Accuracy for Atoms, Molecules, and Solids. *J. Chem. Theory Comput.* **2016**, *12*, 1280–1293.

(13) Zhao, Y.; Schultz, N. E.; Truhlar, D. G. Exchange-correlation functional with broad accuracy for metallic and nonmetallic compounds, kinetics, and noncovalent interactions. *J. Chem. Phys.* **2005**, *123*, 161103.

(14) Zhao, Y.; Schultz, N. E.; Truhlar, D. G. Design of Density Functionals by Combining the Method of Constraint Satisfaction with Parametrization for Thermochemistry, Thermochemical Kinetics, and Noncovalent Interactions. *J. Chem. Theory Comput.* **2006**, *2*, 364–382.

(15) Zhao, Y.; Truhlar, D. The M06 suite of density functionals for main group thermochemistry, thermochemical kinetics, noncovalent interactions, excited states, and transition elements: two new functionals and systematic testing of four M06-class functionals and 12 other functionals. *Theor. Chem. Acc.* **2008**, *120*, 215–241.

(16) Zhao, Y.; Truhlar, D. G. Density Functional for Spectroscopy: No Long-Range Self-Interaction Error, Good Performance for Rydberg and Charge-Transfer States, and Better Performance on Average than B3LYP for Ground States. *J. Phys. Chem. A* **2006**, *110*, 13126–13130.

(17) Zhao, Y.; Truhlar, D. G. Exploring the Limit of Accuracy of the Global Hybrid Meta Density Functional for Main-Group Thermochemistry, Kinetics, and Noncovalent Interactions. *J. Chem. Theory Comput.* **2008**, *4*, 1849–1868.

(18) Yu, H. S.; He, X.; Li, S. L.; Truhlar, D. G. MN15: A Kohn-Sham global-hybrid exchange-correlation density functional with broad accuracy for multi-reference and single-reference systems and noncovalent interactions. *Chem. Sci.* **2016**, *7*, 5032–5051.

(19) Peverati, R.; Truhlar, D. G. Improving the Accuracy of Hybrid Meta-GGA Density Functionals by Range Separation. *J. Phys. Chem. Lett.* **2011**, *2*, 2810–2817.

(20) Peverati, R.; Truhlar, D. G. Screened-exchange density functionals with broad accuracy for chemistry and solid-state physics. *Phys. Chem. Chem. Phys.* **2012**, *14*, 16187–16191.

(21) Schultz, N. E.; Zhao, Y.; Truhlar, D. G. Density Functionals for Inorganometallic and Organometallic Chemistry. *J. Phys. Chem. A* **2005**, *109*, 11127–11143.

(22) Johnson, E. R.; Mori-Sánchez, P.; Cohen, A. J.; Yang, W. Delocalization errors in density functionals and implications for main-group thermochemistry. *J. Chem. Phys.* **2008**, *129*, 204112.

(23) Becke, A. D. Density-functional thermochemistry. V. Systematic optimization of exchange-correlation functionals. *J. Chem. Phys.* **1997**, *107*, 8554–8560.

(24) Peverati, R.; Truhlar, D. G. Quest for a universal density functional: the accuracy of density functionals across a broad spectrum of databases in chemistry and physics. *Phil. Trans. R. Soc. A* **2014**, *372*, 1–52.

(25) Becke, A. D. Simulation of delocalized exchange by local density functionals. *J. Chem. Phys.* **2000**, *112*, 4020–4026.

(26) Becke, A. D. Correlation energy of an inhomogeneous electron gas: A coordinate-space model. *J. Chem. Phys.* **1988**, *88*, 1053–1062.

(27) Voorhis, T. V.; Scuseria, G. E. A novel form for the exchange-correlation energy functional. *J. Chem. Phys.* **1998**, *109*, 400–410.

(28) Hammer, B.; Hansen, L. B.; Nørskov, J. K. Improved adsorption energetics within density-functional theory using revised Perdew-Burke-Ernzerhof functionals. *Phys. Rev. B* **1999**, *59*, 7413–7421.

(29) Stoll, H.; Golka, E.; Preuß, H. Correlation energies in the spin-density functional formalism. *Theor. Chem. Acc.* **1980**, *55*, 29–41.

(30) Perdew, J. P.; Wang, Y. Accurate and simple analytic representation of the electron-gas correlation energy. *Phys. Rev. B* **1992**, *45*, 13244–13249.

(31) Krukau, A. V.; Vydrov, O. A.; Izmaylov, A. F.; Scuseria, G. E. Influence of the exchange screening parameter on the performance of screened hybrid functionals. *J. Chem. Phys.* **2006**, *125*, 224106.

(32) Gill, P. M.; Johnson, B. G.; Pople, J. A. A standard grid for density functional calculations. *Chem. Phys. Lett.* **1993**, *209*, 506 – 512.

(33) Vydrov, O. A.; Voorhis, T. V. Nonlocal van der Waals density functional: The simpler the better. *J. Chem. Phys.* **2010**, *133*, 244103.

(34) Thom H. Dunning, J. Gaussian basis sets for use in correlated molecular calculations. I. The atoms boron through neon and hydrogen. *J. Chem. Phys.* **1989**, *90*, 1007–1023.

(35) Kendall, R. A.; Thom H. Dunning, J.; Harrison, R. J. Electron affinities of the first-row atoms revisited. Systematic basis sets and wave functions. *J. Chem. Phys.* **1992**, *96*, 6796–6806.

(36) Woon, D. E.; Thom H. Dunning, J. Gaussian basis sets for use in correlated molecular calculations. III. The atoms aluminum through argon. *J. Chem. Phys.* **1993**, *98*, 1358–1371.

(37) Jensen, F. Polarization consistent basis sets: Principles. *J. Chem. Phys.* **2001**, *115*, 9113–9125.

(38) Jensen, F. Polarization consistent basis sets. II. Estimating the Kohn–Sham basis set limit. *J. Chem. Phys.* **2002**, *116*, 7372–7379.

(39) Jensen, F. Polarization consistent basis sets. III. The importance of diffuse functions. *J. Chem. Phys.* **2002**, *117*, 9234–9240.

(40) Schäfer, A.; Horn, H.; Ahlrichs, R. Fully optimized contracted Gaussian basis sets for atoms Li to Kr. *J. Chem. Phys.* **1992**, *97*, 2571–2577.

(41) Schäfer, A.; Huber, C.; Ahlrichs, R. Fully optimized contracted Gaussian basis sets of triple zeta valence quality for atoms Li to Kr. *J. Chem. Phys.* **1994**, *100*, 5829–5835.

(42) Weigend, F.; Furche, F.; Ahlrichs, R. Gaussian basis sets of quadruple zeta valence quality for atoms H–Kr. *J. Chem. Phys.* **2003**, *119*, 12753–12762.

(43) Weigend, F.; Ahlrichs, R. Balanced basis sets of split valence, triple zeta valence and quadruple zeta valence quality for H to Rn: Design and assessment of accuracy. *Phys. Chem. Chem. Phys.* **2005**, *7*, 3297–3305.

(44) Rappoport, D.; Furche, F. Property-optimized Gaussian basis sets for molecular response calculations. *J. Chem. Phys.* **2010**, *133*, 134105.

(45) Shao, Y.; Gan, Z.; Epifanovsky, E.; Gilbert, A. T. B.; Wormit, M.; Kussmann, J.; Lange, A. W.; Behn, A.; Deng, J.; Feng, X. et al. Advances in molecular quantum chemistry contained in the Q-Chem 4 program package. *Mol. Phys.* **2015**, *113*, 184–215.

(46) Řezáč, J.; Hobza, P. Describing Noncovalent Interactions beyond the Common Approximations: How Accurate Is the Gold Standard CCSD(T) at the Complete Basis Set Limit? *J. Chem. Theory Comput.* **2013**, *9*, 2151–2155.

(47) Mintz, B. J.; Parks, J. M. Benchmark Interaction Energies for Biologically Relevant Noncovalent Complexes Containing Divalent Sulfur. *J. Phys. Chem. A* **2012**, *116*, 1086–1092.

(48) Řezáč, J.; Hobza, P. Advanced Corrections of Hydrogen Bonding and Dispersion for Semiempirical Quantum Mechanical Methods. *J. Chem. Theory Comput.* **2012**, *8*, 141–151.

(49) Faver, J. C.; Benson, M. L.; He, X.; Roberts, B. P.; Wang, B.; Marshall, M. S.; Kennedy, M. R.; Sherrill, C. D.; Merz, K. M. Formal Estimation of Errors in Computed Absolute Interaction Energies of Protein–Ligand Complexes. *J. Chem. Theory Comput.* **2011**, *7*, 790–797.

(50) Marshall, M. S.; Burns, L. A.; Sherrill, C. D. Basis set convergence of the coupled-cluster correction, $\delta_{MP2}^{CCSD(T)}$: Best practices for benchmarking noncovalent interactions and the attendant revision of the S22, NBC10, HBC6, and HSG databases. *J. Chem. Phys.* **2011**, *135*, 194102.

(51) Hohenstein, E. G.; Sherrill, C. D. Effects of Heteroatoms on Aromatic π–π Interactions: Benzene–Pyridine and Pyridine Dimer. *J. Phys. Chem. A* **2009**, *113*, 878–886.

(52) Sherrill, C. D.; Takatani, T.; Hohenstein, E. G. An Assessment of Theoretical Methods for Nonbonded Interactions: Comparison to Complete Basis Set Limit Coupled-Cluster Potential Energy Curves for the Benzene Dimer, the Methane Dimer, Benzene–Methane, and Benzene–H_2S. *J. Phys. Chem. A* **2009**, *113*, 10146–10159.

(53) Takatani, T.; David Sherrill, C. Performance of spin-component-scaled Møller-Plesset theory (SCS-MP2) for potential energy curves of noncovalent interactions. *Phys. Chem. Chem. Phys.* **2007**, *9*, 6106–6114.

(54) Jurečka, P.; Šponer, J.; Černý, J.; Hobza, P. Benchmark database of accurate (MP2 and CCSD(T) complete basis set limit) interaction energies of small model complexes, DNA base pairs, and amino acid pairs. *Phys. Chem. Chem. Phys.* **2006**, *8*, 1985–1993.

(55) Řezáč, J.; Riley, K. E.; Hobza, P. Benchmark Calculations of Noncovalent In-

teractions of Halogenated Molecules. *J. Chem. Theory Comput.* **2012**, *8*, 4285–4292.

(56) Witte, J.; Goldey, M.; Neaton, J. B.; Head-Gordon, M. Beyond Energies: Geometries of Nonbonded Molecular Complexes as Metrics for Assessing Electronic Structure Approaches. *J. Chem. Theory Comput.* **2015**, *11*, 1481–1492.

(57) Crittenden, D. L. A Systematic CCSD(T) Study of Long-Range and Noncovalent Interactions between Benzene and a Series of First- and Second-Row Hydrides and Rare Gas Atoms. *J. Phys. Chem. A* **2009**, *113*, 1663–1669.

(58) Copeland, K. L.; Tschumper, G. S. Hydrocarbon/Water Interactions: Encouraging Energetics and Structures from DFT but Disconcerting Discrepancies for Hessian Indices. *J. Chem. Theory Comput.* **2012**, *8*, 1646–1656.

(59) Smith, D. G. A.; Jankowski, P.; Slawik, M.; Witek, H. A.; Patkowski, K. Basis Set Convergence of the Post-CCSD(T) Contribution to Noncovalent Interaction Energies. *J. Chem. Theory Comput.* **2014**, *10*, 3140–3150.

(60) Řezáč, J.; Riley, K. E.; Hobza, P. S66: A Well-balanced Database of Benchmark Interaction Energies Relevant to Biomolecular Structures. *J. Chem. Theory Comput.* **2011**, *7*, 2427–2438.

(61) Řezáč, J.; Riley, K. E.; Hobza, P. Extensions of the S66 Data Set: More Accurate Interaction Energies and Angular-Displaced Nonequilibrium Geometries. *J. Chem. Theory Comput.* **2011**, *7*, 3466–3470.

(62) Řezáč, J.; Huang, Y.; Hobza, P.; Beran, G. J. O. Benchmark Calculations of Three-Body Intermolecular Interactions and the Performance of Low-Cost Electronic Structure Methods. *J. Chem. Theory Comput.* **2015**, *11*, 3065–3079.

(63) Granatier, J.; Pitoňák, M.; Hobza, P. Accuracy of Several Wave Function and Density Functional Theory Methods for Description of Noncovalent Interaction of Saturated and Unsaturated Hydrocarbon Dimers. *J. Chem. Theory Comput.* **2012**, *8*, 2282–2292.

(64) Li, S.; Smith, D. G. A.; Patkowski, K. An accurate benchmark description of the interactions between carbon dioxide and polyheterocyclic aromatic compounds containing nitrogen. *Phys. Chem. Chem. Phys.* **2015**, *17*, 16560–16574.

(65) Boese, A. D. Assessment of Coupled Cluster Theory and more Approximate Methods for Hydrogen Bonded Systems. *J. Chem. Theory Comput.* **2013**, *9*, 4403–4413.

(66) Boese, A. D. Basis set limit coupled-cluster studies of hydrogen-bonded systems. *Mol. Phys.* **2015**, *113*, 1618–1629.

(67) Boese, A. D. Density Functional Theory and Hydrogen Bonds: Are We There Yet? *ChemPhysChem* **2015**, *16*, 978–985.

(68) Lao, K. U.; Schäffer, R.; Jansen, G.; Herbert, J. M. Accurate Description of Intermolecular Interactions Involving Ions Using Symmetry-Adapted Perturbation Theory. *J. Chem. Theory Comput.* **2015**, *11*, 2473–2486.

(69) Lao, K. U.; Herbert, J. M. An improved treatment of empirical dispersion and a many-body energy decomposition scheme for the explicit polarization plus symmetry-adapted perturbation theory (XSAPT) method. *J. Chem. Phys.* **2013**, *139*, 034107.

(70) Lao, K. U.; Herbert, J. M. Accurate and Efficient Quantum Chemistry Calculations for Noncovalent Interactions in Many-Body Systems: The XSAPT Family of Methods. *J. Phys. Chem. A* **2015**, *119*, 235–252.

(71) Temelso, B.; Archer, K. A.; Shields, G. C. Benchmark Structures and Binding Energies of Small Water Clusters with Anharmonicity Corrections. *J. Phys. Chem. A* **2011**, *115*, 12034–12046.

(72) Mardirossian, N.; Lambrecht, D. S.; McCaslin, L.; Xantheas, S. S.; Head-Gordon, M. The Performance of Density Functionals for Sulfate–Water Clusters. *J. Chem. Theory Comput.* **2013**, *9*, 1368–1380.

(73) Bryantsev, V. S.; Diallo, M. S.; van Duin, A. C. T.; Goddard, W. A. Evaluation of B3LYP, X3LYP, and M06-Class Density Functionals for Predicting the Binding Energies of Neutral, Protonated, and Deprotonated Water Clusters. *J. Chem. Theory Comput.* **2009**, *5*, 1016–1026.

(74) Goerigk, L.; Grimme, S. A General Database for Main Group Thermochemistry, Kinetics, and Noncovalent Interactions – Assessment of Common and Reparameterized (meta-)GGA Density Functionals. *J. Chem. Theory Comput.* **2010**, *6*, 107–126.

(75) Karton, A.; O'Reilly, R. J.; Chan, B.; Radom, L. Determination of Barrier Heights for Proton Exchange in Small Water, Ammonia, and Hydrogen Fluoride Clusters with G4(MP2)-Type, MPn, and SCS-MPn Procedures–A Caveat. *J. Chem. Theory Comput.* **2012**, *8*, 3128–3136.

(76) Chan, B.; Gilbert, A. T. B.; Gill, P. M. W.; Radom, L. Performance of Density Functional Theory Procedures for the Calculation of Proton-Exchange Barriers: Unusual Behavior of M06-Type Functionals. *J. Chem. Theory Comput.* **2014**, *10*, 3777–3783.

(77) Fanourgakis, G. S.; Aprà, E.; Xantheas, S. S. High-level ab initio calculations for the four low-lying families of minima of $(H_2O)_{20}$. I. Estimates of MP2/CBS binding energies and comparison with empirical potentials. *J. Chem. Phys.* **2004**, *121*, 2655–2663.

(78) Anacker, T.; Friedrich, J. New accurate benchmark energies for large water clusters: DFT is better than expected. *J. Comput. Chem.* **2014**, *35*, 634–643.

(79) Tentscher, P. R.; Arey, J. S. Binding in Radical-Solvent Binary Complexes: Benchmark Energies and Performance of Approximate Methods. *J. Chem. Theory Comput.* **2013**, *9*, 1568–1579.

(80) Kozuch, S.; Martin, J. M. L. Halogen Bonds: Benchmarks and Theoretical Analysis. *J. Chem. Theory Comput.* **2013**, *9*, 1918–1931.

(81) Bauzá, A.; Alkorta, I.; Frontera, A.; Elguero, J. On the Reliability of Pure and Hybrid DFT Methods for the Evaluation of Halogen, Chalcogen, and Pnicogen Bonds Involving Anionic and Neutral Electron Donors. *J. Chem. Theory Comput.* **2013**, *9*, 5201–5210.

(82) de-la Roza, A. O.; Johnson, E. R.; DiLabio, G. A. Halogen Bonding from Dispersion-Corrected Density-Functional Theory: The Role of Delocalization Error. *J. Chem. Theory Comput.* **2014**, *10*, 5436–5447.

(83) Steinmann, S. N.; Piemontesi, C.; Delachat, A.; Corminboeuf, C. Why are the Interaction Energies of Charge-Transfer Complexes Challenging for DFT? *J. Chem. Theory Comput.* **2012**, *8*, 1629–1640.

(84) Karton, A.; Gruzman, D.; Martin, J. M. L. Benchmark Thermochemistry of the C_nH_{2n+2} Alkane Isomers (n = 2–8) and Performance of DFT and Composite Ab Initio Methods for Dispersion-Driven Isomeric Equilibria. *J. Phys. Chem. A* **2009**, *113*, 8434–8447.

(85) Kozuch, S.; Bachrach, S. M.; Martin, J. M. L. Conformational Equilibria in

Butane-1,4-diol: A Benchmark of a Prototypical System with Strong Intramolecular H-bonds. *J. Phys. Chem. A* **2014**, *118*, 293–303.

(86) Gruzman, D.; Karton, A.; Martin, J. M. L. Performance of Ab Initio and Density Functional Methods for Conformational Equilibria of C_nH_{2n+2} Alkane Isomers (n = 4–8). *J. Phys. Chem. A* **2009**, *113*, 11974–11983.

(87) Wilke, J. J.; Lind, M. C.; Schaefer, H. F.; Csaszar, A. G.; Allen, W. D. Conformers of Gaseous Cysteine. *J. Chem. Theory Comput.* **2009**, *5*, 1511–1523.

(88) Martin, J. M. L. What Can We Learn about Dispersion from the Conformer Surface of n-Pentane? *J. Phys. Chem. A* **2013**, *117*, 3118–3132.

(89) Yoo, S.; Aprà, E.; Zeng, X. C.; Xantheas, S. S. High-Level Ab Initio Electronic Structure Calculations of Water Clusters $(H_2O)_{16}$ and $(H_2O)_{17}$: A New Global Minimum for $(H_2O)_{16}$. *J. Phys. Chem. Lett.* **2010**, *1*, 3122–3127.

(90) Fogueri, U. R.; Kozuch, S.; Karton, A.; Martin, J. M. L. The Melatonin Conformer Space: Benchmark and Assessment of Wave Function and DFT Methods for a Paradigmatic Biological and Pharmacological Molecule. *J. Phys. Chem. A* **2013**, *117*, 2269–2277.

(91) Kesharwani, M. K.; Karton, A.; Martin, J. M. L. Benchmark ab Initio Conformational Energies for the Proteinogenic Amino Acids through Explicitly Correlated Methods. Assessment of Density Functional Methods. *J. Chem. Theory Comput.* **2016**, *12*, 444–454.

(92) Yu, L.-J.; Sarrami, F.; Karton, A.; O'Reilly, R. J. An assessment of theoretical procedures for π-conjugation stabilisation energies in enones. *Mol. Phys.* **2015**, *113*, 1284–1296.

(93) Karton, A.; Martin, J. M. L. Explicitly correlated benchmark calculations on C_8H_8 isomer energy separations: how accurate are DFT, double-hybrid, and composite ab initio procedures? *Mol. Phys.* **2012**, *110*, 2477–2491.

(94) Yu, L.-J.; Karton, A. Assessment of theoretical procedures for a diverse set of isomerization reactions involving double-bond migration in conjugated dienes. *Chem. Phys.* **2014**, *441*, 166 – 177.

(95) Karton, A.; Daon, S.; Martin, J. M. L. W4-11: A high-confidence benchmark dataset for computational thermochemistry derived from first-principles W4 data. *Chem. Phys. Lett.* **2011**, *510*, 165 – 178.

(96) Manna, D.; Martin, J. M. L. What Are the Ground State Structures of C_{20} and C_{24}? An Explicitly Correlated Ab Initio Approach. *J. Phys. Chem. A* **2016**, *120*, 153–160.

(97) Curtiss, L. A.; Raghavachari, K.; Trucks, G. W.; Pople, J. A. Gaussian-2 theory for molecular energies of first- and second-row compounds. *J. Chem. Phys.* **1991**, *94*, 7221–7230.

(98) Zhao, Y.; González-García, N.; Truhlar, D. G. Benchmark Database of Barrier Heights for Heavy Atom Transfer, Nucleophilic Substitution, Association, and Unimolecular Reactions and Its Use to Test Theoretical Methods. *J. Phys. Chem. A* **2005**, *109*, 2012–2018.

(99) Zhao, Y.; Lynch, B. J.; Truhlar, D. G. Multi-coefficient extrapolated density functional theory for thermochemistry and thermochemical kinetics. *Phys. Chem. Chem. Phys.* **2005**, *7*, 43–52.

(100) Lynch, B. J.; Zhao, Y.; Truhlar, D. G. Effectiveness of Diffuse Basis Functions for Calculating Relative Energies by Density Functional Theory. *J. Phys. Chem. A* **2003**, *107*, 1384–1388.

(101) Grimme, S.; Kruse, H.; Goerigk, L.; Erker, G. The Mechanism of Dihydrogen Activation by Frustrated Lewis Pairs Revisited. *Angew. Chem. Int. Ed.* **2010**, *49*, 1402–1405.

(102) Goerigk, L.; Grimme, S. Efficient and Accurate Double-Hybrid-Meta-GGA Density Functionals–Evaluation with the Extended GMTKN30 Database for General Main Group Thermochemistry, Kinetics, and Noncovalent Interactions. *J. Chem. Theory Comput.* **2011**, *7*, 291–309.

(103) Krieg, H.; Grimme, S. Thermochemical benchmarking of hydrocarbon bond separation reaction energies: Jacob's ladder is not reversed! *Mol. Phys.* **2010**, *108*, 2655–2666.

(104) O'Reilly, R. J.; Karton, A. A dataset of highly accurate homolytic N–Br bond dissociation energies obtained by Means of W2 theory. *Int. J. Quantum Chem.* **2016**, *116*, 52–60.

(105) Karton, A.; O'Reilly, R. J.; Radom, L. Assessment of Theoretical Procedures for Calculating Barrier Heights for a Diverse Set of Water-Catalyzed Proton-Transfer Reactions. *J. Phys. Chem. A* **2012**, *116*, 4211–4221.

(106) Karton, A.; Schreiner, P. R.; Martin, J. M. L. Heats of formation of platonic hydrocarbon cages by means of high-level thermochemical procedures. *J. Comput. Chem.* **2016**, *37*, 49–58.

(107) Karton, A.; Goerigk, L. Accurate reaction barrier heights of pericyclic reactions: Surprisingly large deviations for the CBS-QB3 composite method and their consequences in DFT benchmark studies. *J. Comput. Chem.* **2015**, *36*, 622–632.

(108) Yu, L.-J.; Sarrami, F.; O'Reilly, R. J.; Karton, A. Reaction barrier heights for cycloreversion of heterocyclic rings: An Achilles' heel for DFT and standard ab initio procedures. *Chem. Phys.* **2015**, *458*, 1 – 8.

(109) Zheng, J.; Zhao, Y.; Truhlar, D. G. Representative Benchmark Suites for Barrier Heights of Diverse Reaction Types and Assessment of Electronic Structure Methods for Thermochemical Kinetics. *J. Chem. Theory Comput.* **2007**, *3*, 569–582.

(110) Karton, A.; Tarnopolsky, A.; Lamère, J.-F.; Schatz, G. C.; Martin, J. M. L. Highly Accurate First-Principles Benchmark Data Sets for the Parametrization and Validation of Density Functional and Other Approximate Methods. Derivation of a Robust, Generally Applicable, Double-Hybrid Functional for Thermochemistry and Thermochemical Kinetics. *J. Phys. Chem. A* **2008**, *112*, 12868–12886.

(111) Yu, L.-J.; Sarrami, F.; O'Reilly, R. J.; Karton, A. Can DFT and ab initio methods describe all aspects of the potential energy surface of cycloreversion reactions? *Mol. Phys.* **2016**, *114*, 21–33.

(112) Chakravorty, S. J.; Gwaltney, S. R.; Davidson, E. R.; Parpia, F. A.; Fischer, C. F. Ground-state correlation energies for atomic ions with 3 to 18 electrons. *Phys. Rev. A* **1993**, *47*, 3649–3670.

(113) Tang, K. T.; Toennies, J. P. The van der Waals potentials between all the rare gas atoms from He to Rn. *J. Chem. Phys.* **2003**, *118*, 4976–4983.

(114) Zheng, J.; Truhlar, D. G. Kinetics of hydrogen-transfer isomerizations of butoxyl radicals. *Phys. Chem. Chem. Phys.* **2010**, *12*, 7782–7793.

(115) Alecu, I. M.; Truhlar, D. G. Computational Study of the Reactions of Methanol with the Hydroperoxyl and Methyl Radicals. 1. Accurate Thermochemistry and Barrier Heights. *J. Phys. Chem. A* **2011**, *115*, 2811–2829.

(116) Seal, P.; Papajak, E.; Truhlar, D. G. Kinetics of the Hydrogen Abstraction from Carbon-3 of 1-Butanol by Hydroperoxyl Radical: Multi-Structural Variational Transition-State Calculations of a Reaction with 262 Conformations of the Transition State. *J. Phys. Chem. Lett.* **2012**, *3*, 264–271.

(117) Seal, P.; Oyedepo, G.; Truhlar, D. G. Kinetics of the Hydrogen Atom Abstraction Reactions from 1-Butanol by Hydroxyl Radical: Theory Matches Experiment and More. *J. Phys. Chem. A* **2013**, *117*, 275–282.

(118) Bao, J. L.; Sripa, P.; Truhlar, D. G. Path-dependent variational effects and multi-dimensional tunneling in multi-path variational transition state theory: rate constants calculated for the reactions of HO_2 with *tert*-butanol by including all 46 paths for abstraction at C and all six paths for abstraction at O. *Phys. Chem. Chem. Phys.* **2016**, *18*, 1032–1041.

(119) Grafenstein, J.; Izotov, D.; Cremer, D. Avoiding singularity problems associated with meta-GGA (generalized gradient approximation) exchange and correlation functionals containing the kinetic energy density. *J. Chem. Phys.* **2007**, *127*, 214103.

(120) Johnson, E. R.; Becke, A. D.; Sherrill, C. D.; DiLabio, G. A. Oscillations in meta-generalized-gradient approximation potential energy surfaces for dispersion-bound complexes. *J. Chem. Phys.* **2009**, *131*, 034111.

(121) Wheeler, S. E.; Houk, K. N. Integration Grid Errors for Meta-GGA-Predicted Reaction Energies: Origin of Grid Errors for the M06 Suite of Functionals. *J. Chem. Theory Comput.* **2010**, *6*, 395–404.

(122) Mardirossian, N.; Head-Gordon, M. ωB97X-V: A 10-parameter, range-separated hybrid, generalized gradient approximation density functional with nonlocal correlation, designed by a survival-of-the-fittest strategy. *Phys. Chem. Chem. Phys.* **2014**, *16*, 9904–9924.

(123) Mardirossian, N.; Head-Gordon, M. Mapping the genome of meta-generalized gradient approximation density functionals: The search for B97M-V. *J. Chem. Phys.* **2015**, *142*, 074111.

(124) Goerigk, L. Treating London-Dispersion Effects with the Latest Minnesota Density Functionals: Problems and Possible Solutions. *J. Phys. Chem. Lett.* **2015**, *6*, 3891–3896.

(125) Witte, J.; Neaton, J. B.; Head-Gordon, M. Push it to the limit: Characterizing the convergence of common sequences of basis sets for intermolecular interactions as described by density functional theory. *J. Chem. Phys.* **2016**, *144*, 194306.

(126) Mardirossian, N.; Head-Gordon, M. ωB97M-V: A combinatorially optimized, range-separated hybrid, meta-GGA density functional with VV10 nonlocal correlation. *J. Chem. Phys.* **2016**, *144*, 214110.

(127) Grimme, S.; Antony, J.; Ehrlich, S.; Krieg, H. A consistent and accurate ab initio parametrization of density functional dispersion correction (DFT-D) for the 94 elements H-Pu. *J. Chem. Phys.* **2010**, *132*, 154104.

(128) Grimme, S.; Ehrlich, S.; Goerigk, L. Effect of the damping function in dispersion corrected density functional theory. *J. Comput. Chem.* **2011**, *32*, 1456–1465.

(129) Schröder, H.; Creon, A.; Schwabe, T. Reformulation of the D3(Becke–Johnson) Dispersion Correction without Resorting to Higher than C_6 Dispersion Coefficients. *J. Chem. Theory Comput.* **2015**, *11*, 3163–3170.

(130) Chai, J.-D.; Head-Gordon, M. Long-range corrected hybrid density functionals with damped atom-atom dispersion corrections. *Phys. Chem. Chem. Phys.* **2008**, *10*, 6615–6620.

(131) Sun, J.; Haunschild, R.; Xiao, B.; Bulik, I. W.; Scuseria, G. E.; Perdew, J. P. Semilocal and hybrid meta-generalized gradient approximations based on the understanding of the kinetic-energy-density dependence. *J. Chem. Phys.* **2013**, *138*, 044113.

(132) Lin, Y.-S.; Li, G.-D.; Mao, S.-P.; Chai, J.-D. Long-Range Corrected Hybrid Density Functionals with Improved Dispersion Corrections. *J. Chem. Theory Comput.* **2013**, *9*, 263–272.

(133) Sun, J.; Ruzsinszky, A.; Perdew, J. P. Strongly Constrained and Appropriately Normed Semilocal Density Functional. *Phys. Rev. Lett.* **2015**, *115*, 036402.

(134) Zhang, Y.; Yang, W. Comment on "Generalized Gradient Approximation Made Simple". *Phys. Rev. Lett.* **1998**, *80*, 890–890.

(135) Vosko, S. H.; Wilk, L.; Nusair, M. Accurate spin-dependent electron liquid correlation energies for local spin density calculations: a critical analysis. *Can. J. Phys.* **1980**, *58*, 1200–1211.

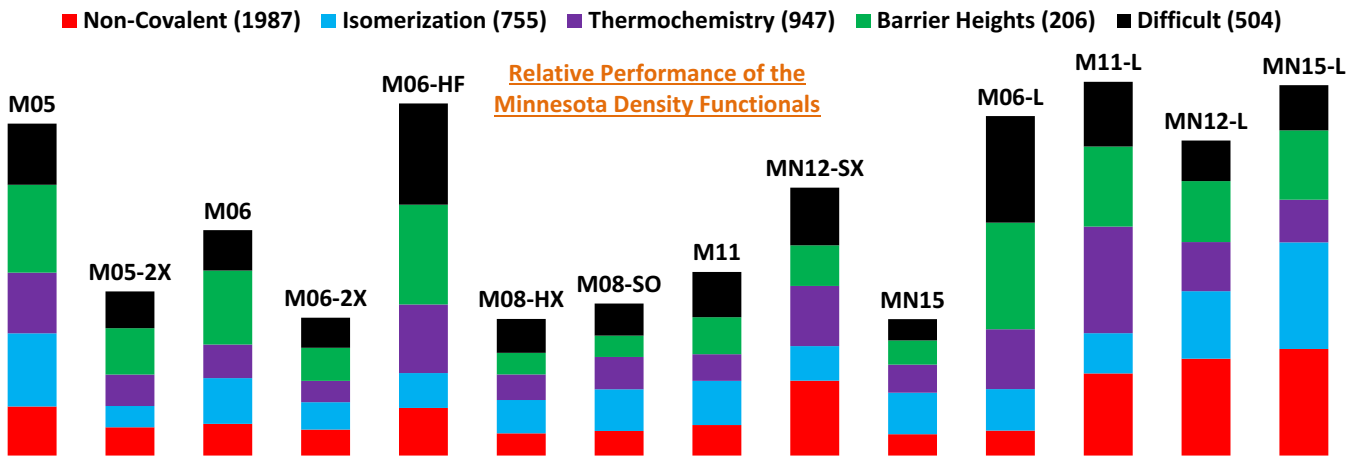

Figure 6: For Table of Contents Use Only